Climate velocities and lagged species elevational shifts in mountain ranges

Sheng-Feng Shen (shensf@sinica.edu.tw)
Academia Sinica https://orcid.org/0000-0002-0631-6343
Wei-Ping Chan
Harvard University
Hung-Chi Kuo
National Taiwan University
I-Ching Chen
National Cheng Kung University https://orcid.org/0000-0002-1909-7290

Biological Sciences - Article

Keywords: climate-endangered endemic species, mountain rangers

Posted Date: January 15th, 2021

DOI: https://doi.org/10.21203/rs.3.rs-108322/v1

For submission to *Nature*

Climate velocities and lagged species elevational shifts in mountain ranges

Authors: Wei-Ping Chan[1,2,3], Hung-Chi Kuo[4] I-Ching Chen[5]* and Sheng-Feng Shen[1]*

Affiliations:

[1]Biodiversity Research Center, Academia Sinica, Taipei, 11529, Taiwan
[2]Department of Organismic and Evolutionary Biology, Harvard University, Cambridge, MA 02138, USA
[3]Bachelor Program in Data Science and Management, Taipei Medical University, Taipei, 106, Taiwan
[4]Department of Atmospheric Sciences, National Taiwan University, Taipei, 10617, Taiwan
[5]Department of Life Sciences, National Cheng Kung University, Tainan, 70101, Taiwan

*Correspondence to:

Sheng-Feng Shen Email: shensf@sinica.edu.tw

I-Ching Chen Email: chenic@mail.ncku.edu.tw

Abstract

Mountain ranges support concentrations of climate-endangered endemic species, and are potential refugia for species retreating from the lowlands under anthropogenic climate change. Predicting the outcome for biodiversity requires knowledge of whether species are shifting uphill at the same rate as temperature isotherms (i.e. whether they are successfully tracking the velocity of climatic changes)[1]. Here, we provide a global assessment of the velocity of climate change in mountain ranges: applying thermal dynamic theory, deriving moist adiabatic lapse rates (MALR) using local surface temperature and water vapor. MALR varied substantially around the world, from 3 to 9°C cooling per km elevation increase. Consider the rate of terrestrial surface warming from 1971 to 2015, 24 regions can be identified as exhibiting high velocities where the isotherms have shifted more than one standard deviation of the global mean value (> 8.45 m yr^{-1}). High velocities are typically found in relatively dry parts of the world, but also occur in wet regions with low lapse rates, such as in Northern Sumatra, Western Guiana Shield, Northern Andes, Costa Rica, Nepal, and Madagascar. Analysis of biodiversity data in relation to mountain-specific velocities revealed more cases of tracking between species and isotherms than previously suggested[2] and more likely occurred at lower climate velocity. Nevertheless, upslope migrations of montane species have generally been lagging behind climate velocity. Such lags could continue to effect change even if the climate were to stabilize immediately. Reducing emissions would be expected to minimize lags, as well as slow the velocities of warming and required responses everywhere.

Main text

Mountainous regions represent 25 % of the Earth's land surface but harbor disproportionately rich biodiversity, due in part to their steep climatic gradients and complex topography[3,4]. Thus, assessing the responses of montane biotas to anthropogenic climate change is particularly important for species conservation. Uphill movements of species towards cooler climates have been widely observed around the globe[2,5-9] yet whether species are keeping pace with shifting climates remains unclear. The sparsity of meteorological stations in many mountain ranges[10], combined with the climatic heterogeneity of complex topographies, make it difficult to determine the 'expected' responses of species if they were track climatic changes precisely. The simplest approach, which we adopt here, is to quantify the magnitude of climate isotherm shifts (i.e. the velocity of climate change) in each mountain range, and then estimate differences between observed range changes and isotherm shifts[1,9,11-15]. We find that uphill movements are generally lagging behind climates and species have no opportunity to track climate effectively unless the velocity is low.

The velocity of thermal isotherm shifts (in km of elevation yr^{-1}) can be derived by dividing the temperature lapse rate (temperature decrease while ascending altitude, in °C km^{-1}) by the surface temperature change (in °C yr^{-1}). However, lapse rates (i.e. 5.5°C km^{-1} in the tropics or 6.5°C km^{-1} elsewhere) that are widely-applied have been inferred from limited ground observations[2,8]. Actual thermal lapse rates can vary substantially in different regions and this has not been explicitly considered in ecological research. Temperature lapse rate is the decrease of temperature with increasing altitude. The pressure of the air decreases when a parcel of air molecules rises and expands with negligible heat transfer conduction and radiation from outside, which costs internal energy, cooling the parcel. The consequent rate of cooling is referred as adiabatic lapse rate ("adiabatic" meaning that no external source of energy

72 was involved, and the value often used is 9.8°C km^{-1}). However, if the air condenses
73 moisture as it cools, it gains some heat of condensation, which slows the rate of
74 cooling. Thus, realized or "moist adiabatic" lapse rates (MALR) are often lower (e.g.
75 6.5°C km^{-1}) than the adiabatic lapse rate. As a consequence, temperature lapse rates
76 are determined by water vapor changes and latent heat release, which are linked to
77 surface temperature, elevation and moisture content in the region of interest[16].
78 Importantly, the limited data available indicates that temperature lapse rates
79 differ between regions and seasons[16,17]. For example, lapse rates range from 4.1°C
80 km^{-1} to 6.8°C km^{-1} for different times and seasons along the slopes of the central
81 Himalayas[18]. In the Washington Cascades mountains in North America, the values of
82 lapse rates vary from 2.5 km^{-1} to 7.5°C km^{-1} in late summer and spring[19].
83 Nonetheless, the mechanisms underlying temperature lapse rate are well established
84 in thermodynamic theory, with MALR being a function of local temperature and
85 vapor pressure[20]. Here, we use this knowledge to assess the velocity of mountain
86 climate changes on a global scale, and then evaluate whether species are keeping pace
87 with shifting isotherms. Mountain areas were represented by grids with 0.5°
88 resolution of mean elevation above 1,000 m[21] (Figs. 1,2). The velocity is represented
89 by the vertical isotherm shifts (i.e. how far an isothermal line rises from the surface),
90 calculated by dividing the rate of warming in each mountain grid by its MALR,
91 derived from terrain-surface conditions. We estimate MALR (usually noted as Γ_w) as:

92 $$\Gamma_w = g \frac{1 + \frac{H_v \gamma}{R_{sd} T}}{C_{pd} + \frac{H_v^2 \gamma \epsilon}{R_{sd} T^2}}$$

93 where γ is the mixing ratio of the mass of water vapor per unit mass of dry air, which
94 is also influenced by air pressure; T represents the air temperature (other parameters
95 are constants; see Methods). We use mean annual temperature and water vapor

96 pressure at terrain surface from 2011 to 2015 from CRU TS 3.24 to calculate MALR
97 and consider the rate of warming from 1971 to 2015 for each mountain grid. The
98 MALR formula predicts that higher surface temperature or water vapor leads to
99 curvilinear decreases in MALR (Fig. 1a). Given the widely varied temperature and
100 water vapor differences between mountain grids (Fig. 1 b,c), our estimates show that
101 temperature lapse rates of global mountains vary from 3 to 9°C km^{-1} (Fig 1d).
102 Given these MALR estimates and the rates of surface temperature change (Fig. 2
103 a,b), the climate velocities in global mountains vary considerably from -16.67 m yr^{-1}
104 (Saltillo, Mexico) to +16.80 m yr^{-1} (Mashhad, Iran), with global average elevational
105 isotherm increases of +5.42 ± 0.03 m yr^{-1} in mountain ranges (Fig. 2c; Extended Data
106 Fig. 1). We identify high climate-velocity mountains where the isotherms have shifted
107 more than one standard deviation of the global mean value (higher than 8.45 m yr^{-1})
108 (Fig. 2d). Defined in this way, about 16% of mountainous areas are exposed to high
109 climate velocity and many are well-recognized biodiversity hotspots, such as
110 Northern Sumatra, Hengduan, Nepal, Southern Ghats, Madagascar, Mediterranean
111 basin, Northern Sahara, Brazilian Highlands, Northern Andes, Costa Rica, and
112 Western America and Mexico (Supplementary Table 1). Other high velocity
113 mountains may also be of concern, including most of the Middle East mountains
114 (which includes endemics) and central Asia, Siberia, and the Alaska-Yukon region
115 (Supplementary Table 1). The approach delineates that high climate velocity can be
116 due to high rates of temperature warming or to low lapse rates. It is intuitive that
117 higher warming rate results in high climate velocity (Extended Data Fig. 2a) and this
118 is often observed in drier regions with low mean annual precipitation (MAP), possibly
119 due to the limited heat capacity of arid regions[22-24] (Supplementary Table 1). Yet, high
120 climate velocities are also observed in mountain ranges that have relatively modest
121 levels of warming but low lapse rates, which can occur at areas with high water

vapour pressure and/or high surface temperatures (Extended Data Fig. 2b, and Supplementary Table 1). Many of these areas coincide with wet climates (high MAP), such as in Northern Sumatra, Western Guiana Shield, Northern Andes Mts, Costa Rica, and Nepal (Extended Data Fig. 2b, and Supplementary Table 1). Mountain climate velocities emerge from the interactions of lapse rates and water vapor pressure, interacting with mountain topographies and levels of regional warming.

We also applied our framework to mountains on islands that harbor a high proportion of endemic species and provide refuges for shifting species otherwise constrained by the ocean[25,26]. We define islands as landmasses that are smaller than Australia and surrounded by water[21]. We examined the velocity of climate change in island mountains globally (only 14 islands have mountain grid cells higher than 1,000 m, based on our dataset) and found a mean shift of 3.35 m yr^{-1}, which was lower than the global average (5.42 m yr^{-1}). Two island regions—Madagascar and Japan —were found to have high climate velocity (>8.45 m yr^{-1}) (Fig. 3a-c). In Japan, high climate velocity is mainly caused by the surface temperature warming (Fig. 2b, Supplementary Table 1) but, interestingly, Madagascar is not adjacent to ocean with particularly high levels sea surface warming[27] (Fig. 2b, Supplementary Table 1); for Madagascar, high water vapour levels generate a low lapse rate, and hence the high climate velocity (Supplementary Table 1). High climate velocity in these islands may lead to considerable biodiversity loss, which illustrates the importance of developing climate adaptation strategies[28].

Growing evidence shows that the rate of warming varies with elevation[10]. The sparse long-term meteorological stations in mountain areas have hampered a global test of elevation dependent warming[29]. Our study reveals a complex pattern of elevation-dependent climate velocity (Fig. 3d-f and Extended Data Fig. 3).

Accelerated climate velocity with elevation can be observed in the low latitudes (*ca*. 10°N/S) but high velocity occurs mostly at low elevation near the equator and at 30-40°N, 60-70°N and 20-30°S, in line with the projections of the IPCC Fifth Assessment Report[30]. These complex patterns support the call for greater undestanding of the patterns and causes of elevation-dependent warming[10].

Since factors such as whether the slopes face the sun may have a major impact on the mountain climate[31], we further explored how the topography of the mountains, including the aspect and orientation of the mountains, affects climate velocity. We investigate how mountain climate velocities differ among different aspects and orientations. Apart from commonly known North-South and East-West orientations, we further defined two categories: mountains facing east and equator are called East-Equator mountains; facing west and equator, West-Equator mountains (Extended Data Fig. 4a). We found that climate velocities are higher in East-facing and West-facing slopes than other slopes ($\chi^2 = 11.06$, $p = 0.011$, d.f. = 3) (Extended Data Fig. 4b), which are associated with the higher water vapor in these aspects of slopes than the others ($\chi^2 = 687.76$, $p<0.001$, d.f. = 3) (Extended Data Fig. 4c) even though the warming rates were lower than the other slopes ($\chi^2 = 267.62$, $p<0.001$, d.f. = 3) (Extended Data Fig. 4d). Regarding the orientation, climate velocities are significantly higher in East-Equator (orientations illustrated in Extended Data Fig. 4) and North-South mountains than mountain ranges of other orientations ($\chi^2 = 765.72$, $p<0.001$, d.f. = 3) (Extended Data Fig. 4e). Water vapor values are significantly higher in East-Equator mountains ($\chi^2 = 521.72$, $p<0.001$, d.f. = 3, Extended Data Fig. 4f) but surface temperature changes are significantly higher in North-South mountains, compared to East-West and West-Equator mountains (E-W: $z = -9.05$, $p<0.001$; W-Equator: $z = -7.98$, $p<0.001$) (Extended Data Fig. 4g). This observation is generally

consistent in mountain orientations of different aspects (Extended Data Fig. 5).

Our study provides estimates of the rates of elevational shifts required by species and whether they tracked (kept pace with) temperature changes precisely or lagged behind. We compared these rate estimates with observed elevational shifts in montane species, taken from peer-reviewed articles reporting multi-species elevational redistributions (Supplementary Table 2). The global variation in predicted elevation shifts in different mountain ranges shows that rates of expected species uplifts are much lower (e.g. in Italy and France) than predicted in the original paper using widely applied empirical values (range from 5.5°C km^{-1} to 6.5°C km^{-1}) or a globally-averaged lapse rate of 5.5°C km^{-1} (Extended Data Fig. 6), and this may partially explain previous findings that mountain species appeared to be generally lagging behind climate changes[2]. To assess the probability of species tracking climate velocity, considering each taxon at each region as one data-point, we conducted bootstrapping to control the sample size effect and compare the probability of tracking in relation to climate velocity (Fig. 4a). Each dataset was subsampled and the mean shift was compared with its corresponding climate velocity, using Wilcoxon signed-rank test at significance level of 0.05. If the shifts of species are not significantly different from the climate velocity, we consider the species successfully track the climate velocity. We repeated the procedure for 1000 times (i = 1000) and used the percentage of numbers that are not significantly different from the climate velocity as the probability of tracking successfully (Fig. 4b-c; significant levels at p = 0.01 and 0.001 were shown in Fig.4d & 4e). The probability of species tracking thus represents the variation within each data point and provided better assessment than comparing only the mean values of shifts, i.e. data points that are closer to the 1:1 diagnose line are not necessarily tracking better. Plotting the probability of species tracking demonstrated that mountain species are generally lagging behind the climate

200 velocities with exceptions more likely occurring at lower velocities (Fig. 4b, Extended
201 Data Fig. 7).
202 By applying the well-established thermodynamic theory of MALR, we provide a
203 global assessment of climate velocity in mountain ranges and identify 24 major
204 regions with high climate velocities. In addition to dry regions with increasing surface
205 temperatures [32,33], we identify mountains where high water vapor causes high climate
206 velocity. Based on the newly calculated climate velocity, we also evaluate the
207 probability of species tracking climate velocity in global mountains. Many ecological
208 studies rely on average lapse rates collected by the sounding balloon method, tying a
209 thermometer on a balloon in order to collect the temperature profile vertically, to
210 estimate isothermal line shifts in mountain regions. The more accurate estimations of
211 climate velocity provide potential explanations for the largely lagged upslope
212 migrations previously documented in many species. Nevertheless, the biological
213 impacts of climate change have largely been studied in North America and
214 Europe[34,35] , where the velocities of mountain climate change are relatively slower
215 than most other parts of the world. We still have a limited understanding of whether
216 species generally move uphill more slowly than the shift of isothermal lines[9] and, if
217 they do move more slowly, what the ecological impacts of climate change are for
218 these lagging species.
219 Our estimation of global temperature lapse rates, based on the MALR formula
220 considering the latent heat release and water vapor changes, provides a heuristic
221 understanding of climate velocity in global mountains. However, many other
222 mechanisms, such snow albedo, radiative flux changes, surface heat loss and aerosols,
223 also influence the energy balance regimes, making a direct estimate of climate
224 conditions and climate change in extremely difficult in mountain regions[10].
225 Nevertheless, since mountains may effectively provide shelters for many rare and

endangered species, our study helps identify vulnerable regions with high climate velocity, which we suggest are priority regions for conservation. Given this vulnerability, extensive monitoring networks for both mountain climate and biological impacts are urgently needed.

Methods

The climatic data sources and the calculation of MALR

The climatic data, including mean annual temperature and water vapor pressure, and the corresponding global digital elevation model were derived from the gridded CRU TS3.24 database (0.5° resolution), which we averaged over every 5 years. Both mean annual temperature and water vapor pressure were derived from local weather stations and subsequently averaged across coarse spatial extent to obtain the final values [24]. MALR at each grid was generated by the MALR formula:

$$\Gamma_w = g\,\frac{1+\frac{H_v\,\gamma}{R_{sd}\,T}}{C_{pd}+\frac{H_v^2\,\gamma\,\epsilon}{R_{sd}\,T^2}}$$

where Γ_w is the moist adiabatic lapse rate (K/m), g denotes the Earth's gravitational acceleration (9.8076 m/s^2), H_v denotes the heat of water vaporization (2,501,000 J/kg), R_{sd} denotes the specific gas constant of dry air (287 J kg^{-1} K^{-1}), ϵ denotes the dimensionless ratio of the specific gas constant of dry air to the specific gas constant for water vapour (0.622), C_{pd} denotes the specific heat of dry air at constant pressure (1,005 J kg^{-1} K^{-1}), and T denotes the air temperature (K). γ is the mixing ratio of the mass of water vapor to the mass of dry air:

$$\gamma = \epsilon e/(p-e)$$

where e represents the water vapor pressure of the air and p represents the pressure of the air. Here, p was derived from the Barometric formula:

$$p = p_b \times exp\left[\frac{-g \times M \times h}{R \times T}\right]$$

where p_b denotes the static pressure (101,325.00 pascals), M denotes the molar mass of Earth's air (0.0289644 kg/mol), R denotes the universal gas constant for air (8.31432 N m mol^{-1} K^{-1}), h denotes the height above sea level (meters), and T denotes the standard temperature (K).

The preprocessing of climatic variables (from monthly data to annual data) and the calculation of basic climate velocity and climate velocity was computed by pySpark. Islands are defined as landmasses that are smaller than Australia and surrounded by water[21]. Here, the input dataset is not the digital elevation model (DEM) from CRU but from SRTM, which is more conservative on defining terrestrial area (smaller terrestrial regions), so it is better for island detection (the islands near shores are not connected to continents). Greenland is not included as it is not surrounded by the ocean in the dataset. These analyses were run in Wolfram Mathematica 9. Though we only present the results when the anthropogenic warming accelerated (Extended Data Fig. 8) in our main text, the results from 1901 to 2015 can be found in Supplementary Fig. 1 & 2.

Topographical analysis and corresponding data sources

The surface aspect of each pixel was calculated by using the Surface Aspect Tool in ArcGIS Pro (the license of 3D analyst is required), and the input digital elevation model (DEM) is from CRU in order to match the climatic data. Two characters (elongation and orientation) were calculated for each mountain ranges previously defined in the literature[36] in Wolfram Mathematica 9. Elongation is defined as 1-(smallest axis of the best-fit ellipse / largest axis of the best-fit ellipse), and orientation is computed as the angle between the largest axis and the horizontal axis. The orientation of only those mountains having elongation value greater than 0.5 were further analyzed. To provide a better alignment with the definition of global mountains described in the main text, we then analyzed climatic data from elevations higher than 1,000 m (a.s.l.) within these 'expert-identified' mountains. For the clarity, we summarized the results based on categories of surface aspects and orientations of mountains (Extended Data Fig. 4a). Kruskal–Wallis test (non-parametric) was applied

to statistically quantify the differences across different aspects and orientations of mountains. A Wilcoxon signed-rank test was then applied in paired-dataset comparisons as a post Hoc analysis.

Biological datasets

We adapted published studies providing range- or boundary-shift information based on an exhaustive literature review (Supplementary Table 2). Generally, literature was collected based on Chen et al. 2011 and updated to 2017. Investigations of different taxa within the same region were considered as different records (e.g., [37]). Certain records collected during this process were subsequently discarded from the dataset when either: (1) the values returned two different studies in the same region were enormously different, specifically exceeding a ratio of 5 (e.g., in Spain [Sierra Nevada][38], the number of samples in two investigating periods were 1,168 V.S. 29,174); (2) the information provided in a large-scale (exceed 5 x 5 degree on the map) research was insufficient, so we could not divide the records into geographical regions (e.g., [39]). Along with the raw datasets we used in our analysis, statistically summarized information for all literature is also provided. The standard error was not provided for studies with (1) only one record in a region or (2) insufficient information from the original paper.

Corresponding climate velocity to the biological data

To pair biological records with the climate velocity derived from MALR, climate velocities were assigned or statistically summarized based on the following criteria: (1) if the spatial scale of a research was less than 1 x 1 degree (i.e. distributed within a grid), the climate velocity at the same corresponding grid was used (eg. [40]); (2) if the scale of a study exceeded 1 x 1 degree (i.e., distributed on multiple grids), the regional

climate velocity was statistically calculated (provided as mean, variance, and sample size; e.g. [41]); (3) if the study region exceeds 5 x 5 degrees, the biological records were grouped into different regions (e.g. [8]), and the climate velocity of each region was derived based on criteria 1 and 2; (4) for studies encompassing multiple regions and periods, the corresponding spatiotemporal information was used in order to derive the most accurate climate velocity (eg., [42]); (5) if a study investigated the same region multiple times in different temporal periods, the same geographical information was used (e.g. [43]).

The probability of species tracking climate velocity—comparing biological data and climate velocity

In order to statistically compare the biological data with corresponding climate velocity, we calculated the probability of species tracking climate velocity after bootstrapping the data to meet a relatively constant sample size across regions and taxa. Some studies did provide detailed raw data (Supplementary Table 2), but for those only reporting statistical results—such as mean and variance/standard deviation/error (Extended Data Fig. 9)—we applied different probability distribution functions, normal distribution as well as non-normal distributions (log-normal and Student-t distribution), in our statistical analysis according to the statistical characteristics (mean and standard deviation/error) provided in the original reports. The nature of non-normally-distributed frequency in our dataset (Supplementary Fig. 3) was taken cared here, and the final probability reported was averaged from all three approaches with different probabilities.

The probability of species tracking climate velocity was then calculated as follows: First of all, we used the bootstrap technique to subsample the dataset to control the inconsistencies induced by having different sample sizes across studies. For each

taxon in each region, we set the sample size to *n* and drew *n* records (*n* in Fig. 4a). If the total number of records for that taxon in that region is smaller than *n*, all records were used. For those only reporting statistical results (21 out of 47), we applied different probability functions to generate the drawn value as described in the previous paragraph. The drawn biological data were then compared to the corresponding climatic velocity using the non-parametric method—Wilcoxon signed-rank test—because many datasets did not satisfy the normal distributed assumption (Supplementary Fig. 3). This procedure (draw and comparison) was then iterated 1,000 times (*i* in Fig. 4a), and we calculated the number of iterations at which the biological data showed no significant difference to the corresponding climate velocity (i.e., did not meet the significant level, 0.05; *p* in Fig. 4 which implies the ability of tracking climate change; the lower *p*, the higher ability) and divided it by the total number of iterations (1,000; *i* in Fig. 4a); the result was the probability of species tracking climate velocity. A logistic-type (probit) function was then applied to estimate the probability curve. We also ran a sensitivity analysis by setting different values for *n* (30, 40, 50, 60, 70, 80, 90, and 100), and the results indicated that *n* does not influence the probability of species tracking climate velocity (Supplementary Table 3), so we decided to set $n = 30$ to fairly address the small-sample-size research. The data processing and statistical analysis in this section were done in R.

Probability of species tracking using different lapse rate calculations

The straightforward thought to test how better climate velocity derived from MALR (with the consideration of water vapor) is tracked by species should be: applying regression for water vapor and the residual that derived from the regression of biological records and local constant lapse rate (which does not consider water vapor). However, given that the relation between water vapor and lapse rate is non-linear

(MALR formula and Fig. 1a), the analysis based on the concept of regression should not work. In order to bridge the method, which is more familiar to readers, to our formal analysis (which is going to be described later), we firstly provide a set of intuitive but potentially biased histograms to show the different explanation powers among different lapse rate calculations (Extended Data Fig. 10a). The residual between mean observed shifting rate and the mean climate velocity derived from different lapse rate calculations for a taxon are shown. We can still find that the residual histogram of MALR is more normally distributed than that of others (i.e. it explains biological dataset better than others), yet please note that this method neglects the variance of different records of a taxon. Consequently, in order to formally compare different lapse rate calculations, the method with probability scope and subsampling is applied. Based on the results generated from the previous section, we further calculated the averaged probability of species tracking climate velocity (the concept behind this analysis is quite similar to the survival analysis[44]). We sorted the data by ascending climate velocities and then calculated the cumulated probability for each record before dividing it by the cumulated number of records. For example, there are four records (format: probability of species tracking climate velocity, climate velocity): (0.98, 0.2), (0.90, 0.4), (0.75, 0.6), (0.6, 0.7). The averaged probability under a certain climate velocity would then be: (0.98, 0.2), (0.94, 0.4), (0.88, 0.6), (0.81, 0.7). 0.94 is from (0.98+0.90)/2; 0.88 is from (0.98+0.90+0.75)/3; 0.81 is from (0.98+0.90+0.75+0.60)/4. This result can be directly compared to the ultimate impacts of lapse rates derived from different methods (local constant lapse rate, constant lapse rate, and MALR) on the probability of species tracking climate velocity (Extended Data Fig. 10b). The analysis was done in R.

Main References

1 Loarie, S. R. *et al.* The velocity of climate change. *Nature* **462**, 1052-U1111, doi:10.1038/nature08649 (2009).

2 Chen, I.-C., Hill, J. K., Ohlemüller, R., Roy, D. B. & Thomas, C. D. Rapid range shifts of species associated with high levels of climate warming. *Science* **333**, 1024-1026 (2011).

3 Rahbek, C. *et al.* Building mountain biodiversity: Geological and evolutionary processes. *Science* **365**, 1114-1119, doi:10.1126/science.aax0151 (2019).

4 Rahbek, C. *et al.* Humboldt's enigma: What causes global patterns of mountain biodiversity? *Science* **365**, 1108-1113 (2019).

5 Lenoir, J. & Svenning, J. C. Climate-related range shifts–a global multidimensional synthesis and new research directions. *Ecography* **38**, 15-28 (2015).

6 Morueta-Holme, N. *et al.* Strong upslope shifts in Chimborazo's vegetation over two centuries since Humboldt. *P Natl Acad Sci USA* **112**, 12741-12745 (2015).

7 Freeman, B. G., Lee-Yaw, J. A., Sunday, J. M. & Hargreaves, A. L. Expanding, shifting and shrinking: The impact of global warming on species' elevational distributions. *Global Ecol Biogeogr* **27**, 1268-1276 (2018).

8 Freeman, B. G. & Freeman, A. M. C. Rapid upslope shifts in New Guinean birds illustrate strong distributional responses of tropical montane species to global warming. *P Natl Acad Sci USA* **111**, 4490-4494 (2014).

9 Lenoir, J. *et al.* Species better track climate warming in the oceans than on land. *Nature Ecology & Evolution*, 1-16 (2020).

10 Pepin, N. *et al.* Elevation-dependent warming in mountain regions of the world. *Nat Clim Change* **5**, 424-430, doi:10.1038/Nclimate2563 (2015).

11 Brito-Morales, I. *et al.* Climate velocity can inform conservation in a warming world. *Trends in ecology & evolution* **33**, 441-457 (2018).

12 Burrows, M. T. *et al.* The Pace of Shifting Climate in Marine and Terrestrial Ecosystems. *Science* **334**, 652-655, doi:10.1126/science.1210288 (2011).

13 Pinsky, M. L., Worm, B., Fogarty, M. J., Sarmiento, J. L. & Levin, S. A. Marine Taxa Track Local Climate Velocities. *Science* **341**, 1239-1242, doi:10.1126/science.1239352 (2013).

14 Poloczanska, E. S. *et al.* Global imprint of climate change on marine life. *Nat Clim Change* **3**, 919-925, doi:10.1038/Nclimate1958 (2013).

15 Schloss, C. A., Nunez, T. A. & Lawler, J. J. Dispersal will limit ability of mammals to track climate change in the Western Hemisphere. *P Natl Acad Sci USA* **109**, 8606-8611, doi:10.1073/pnas.1116791109 (2012).

16 Stone, P. H. & Carlson, J. H. Atmospheric Lapse Rate Regimes and Their Parameterization. *J Atmos Sci* **36**, 415-423, doi:Doi 10.1175/1520-0469(1979)036<0415:Alrrat>2.0.Co;2 (1979).
17 Meyer, H. W. Lapse rates and other variables applied to estimating paleoaltitudes from fossil floras. *Palaeogeography, Palaeoclimatology, Palaeoecology* **99**, 71-99 (1992).
18 Kattel, D. *et al.* Temperature lapse rate in complex mountain terrain on the southern slope of the central Himalayas. *Theoretical and Applied Climatology* **113**, 671-682 (2013).
19 Minder, J. R., Mote, P. W. & Lundquist, J. D. Surface temperature lapse rates over complex terrain: Lessons from the Cascade Mountains. *Journal of Geophysical Research: Atmospheres* **115** (2010).
20 Holton, J. R. & Hakim, G. J. *An introduction to dynamic meteorology*. Vol. 88 (Academic press, 2012).
21 Kreft, H., Jetz, W., Mutke, J., Kier, G. & Barthlott, W. Global diversity of island floras from a macroecological perspective. *Ecol Lett* **11**, 116-127 (2008).
22 Huang, J., Guan, X. & Ji, F. Enhanced cold-season warming in semi-arid regions. *Atmos Chem Phys* **12**, 5391-5398, doi:10.5194/acp-12-5391-2012 (2012).
23 Huang, J., Yu, H., Guan, X., Wang, G. & Guo, R. Accelerated dryland expansion under climate change. *Nat Clim Change* (2015).
24 Ji, F., Wu, Z. H., Huang, J. P. & Chassignet, E. P. Evolution of land surface air temperature trend. *Nat Clim Change* **4**, 462-466, doi:10.1038/Nclimate2223 (2014).
25 Kier, G. *et al.* A global assessment of endemism and species richness across island and mainland regions. *P Natl Acad Sci USA* **106**, 9322-9327, doi:10.1073/pnas.0810306106 (2009).
26 Veron, S., Mouchet, M., Govaerts, R., Haevermans, T. & Pellens, R. Vulnerability to climate change of islands worldwide and its impact on the tree of life. *Scientific Report* **9**, 14471, doi:10.1038/s41598-019-51107-x (2019).
27 Kenyon, J. & Hegerl, G. C. Influence of modes of climate variability on global temperature extremes. *J Climate* **21**, 3872-3889, doi:Doi 10.1175/2008jcli2125.1 (2008).
28 Courchamp, F., Hoffmann, B. D., Russell, J. C., Leclerc, C. & Bellard, C. Climate change, sea-level rise, and conservation: keeping island biodiversity afloat. *Trends in Ecology & Evolution* **29**, 127-130, doi:10.1016/j.tree.2014.01.001 (2014).

29 Rangwala, I. & Miller, J. R. Climate change in mountains: a review of elevation-dependent warming and its possible causes. *Climatic Change* **114**, 527-547 (2012).

30 Collins, M. *et al.* in *Climate Change 2013-The Physical Science Basis: Contribution of Working Group I to the Fifth Assessment Report of the Intergovernmental Panel on Climate Change* 1029-1136 (Cambridge University Press, 2013).

31 Waring, R. H. & Running, S. W. *Forest ecosystems: analysis at multiple scales*. (Elsevier, 2010).

32 Lioubimtseva, E. & Henebry, G. M. Climate and environmental change in arid Central Asia: Impacts, vulnerability, and adaptations. *J Arid Environ* **73**, 963-977, doi:DOI 10.1016/j.jaridenv.2009.04.022 (2009).

33 Sorg, A., Bolch, T., Stoffel, M., Solomina, O. & Beniston, M. Climate change impacts on glaciers and runoff in Tien Shan (Central Asia). *Nat Clim Change* **2**, 725-731, doi:Doi 10.1038/Nclimate1592 (2012).

34 Pecl, G. T. *et al.* Biodiversity redistribution under climate change: Impacts on ecosystems and human well-being. *Science* **355**, eaai9214 (2017).

35 Pacifici, M. *et al.* Assessing species vulnerability to climate change. *Nat Clim Change* **5**, 215 (2015).

36 Elsen, P. R. & Tingley, M. W. Global mountain topography and the fate of montane species under climate change. *Nat Clim Change* **5**, 772 (2015).

37 Hickling, R., Roy, D. B., Hill, J. K., Fox, R. & Thomas, C. D. The distributions of a wide range of taxonomic groups are expanding polewards. *Global Change Biol* **12**, 450-455 (2006).

38 Menendez, R., Gonzalez-Megias, A., Jay-Robert, P. & Marquez-Ferrando, R. Climate change and elevational range shifts: evidence from dung beetles in two European mountain ranges. *Global Ecol Biogeogr* **23**, 646-657 (2014).

39 Pauli, H. *et al.* Recent Plant Diversity Changes on Europe's Mountain Summits. *Science* **336**, 353-355 (2012).

40 Reif, J. & Flousek, J. The role of species' ecological traits in climatically driven altitudinal range shifts of central European birds. *Oikos* **121**, 1053-1060 (2012).

41 Holzinger, B., Hulber, K., Camenisch, M. & Grabherr, G. Changes in plant species richness over the last century in the eastern Swiss Alps: elevational gradient, bedrock effects and migration rates. *Plant Ecol* **195**, 179-196 (2008).

42 Tingley, M. W., Koo, M. S., Moritz, C., Rush, A. C. & Beissinger, S. R. The push and pull of climate change causes heterogeneous shifts in avian elevational ranges. *Global Change Biol* **18**, 3279-3290 (2012).

43 Jump, A. S., Huang, T. J. & Chou, C. H. Rapid altitudinal migration of mountain plants in Taiwan and its implications for high altitude biodiversity. *Ecography* **35**, 204-210 (2012).
44 Pollock, K. H., Winterstein, S. R., Bunck, C. M. & Curtis, P. D. Survival analysis in telemetry studies: the staggered entry design. *The Journal of Wildlife Management*, 7-15 (1989).
45 Myers, N., Mittermeier, R. A., Mittermeier, C. G., da Fonseca, G. A. B. & Kent, J. Biodiversity hotspots for conservation priorities. *Nature* **403**, 853-858 (2000).
46 Bergamini, A., Ungricht, S. & Hofmann, H. An elevational shift of cryophilous bryophytes in the last century - an effect of climate warming? *Divers Distrib* **15**, 871-879 (2009).
47 Wilson, R. J. *et al.* Changes to the elevational limits and extent of species ranges associated with climate change. *Ecol Lett* **8**, 1138-1146, doi:10.1111/j.1461-0248.2005.00824.x (2005).
48 Raxworthy, C. J. *et al.* Extinction vulnerability of tropical montane endemism from warming and upslope displacement: a preliminary appraisal for the highest massif in Madagascar. *Global Change Biol* **14**, 1703-1720 (2008).
49 Archaux, F. Breeding upwards when climate is becoming warmer: no bird response in the French Alps. *Ibis* **146**, 138-144 (2004).
50 Popy, S., Bordignon, L. & Prodon, R. A weak upward elevational shift in the distributions of breeding birds in the Italian Alps. *J Biogeogr* **37**, 57-67 (2010).
51 Zuckerberg, B., Woods, A. M. & Porter, W. F. Poleward shifts in breeding bird distributions in New York State. *Global Change Biol* **15**, 1866-1883 (2009).
52 Moritz, C. *et al.* Impact of a century of climate change on small-mammal communities in Yosemite National Park, USA. *Science* **322**, 261-264, doi:10.1126/science.1163428 (2008).
53 Parolo, G. & Rossi, G. Upward migration of vascular plants following a climate warming trend in the Alps. *Basic Appl Ecol* **9**, 100-107 (2008).
54 Kelly, A. E. & Goulden, M. L. Rapid shifts in plant distribution with recent climate change. *P Natl Acad Sci USA* **105**, 11823-11826 (2008).
55 Lenoir, J., Gegout, J. C., Marquet, P. A., de Ruffray, P. & Brisse, H. A significant upward shift in plant species optimum elevation during the 20th century. *Science* **320**, 1768-1771 (2008).
56 le Roux, P. C. & McGeoch, M. A. Rapid range expansion and community reorganization in response to warming. *Global Change Biol* **14**, 2950-2962 (2008).
57 Konvicka, M., Maradova, M., Benes, J., Fric, Z. & Kepka, P. Uphill shifts in

distribution of butterflies in the Czech Republic: effects of changing climate detected on a regional scale. *Global Ecol Biogeogr* **12**, 403-410 (2003).
58 Franco, A. M. A. *et al.* Impacts of climate warming and habitat loss on extinctions at species' low-latitude range boundaries. *Global Change Biol* **12**, 1545-1553 (2006).
59 Feeley, K. J. *et al.* Upslope migration of Andean trees. *J Biogeogr* **38**, 783-791 (2011).
60 Forero-Medina, G., Joppa, L. & Pimm, S. L. Constraints to Species' Elevational Range Shifts as Climate Changes. *Conserv Biol* **25**, 163-171 (2011).
61 Felde, V. A., Kapfer, J. & Grytnes, J. A. Upward shift in elevational plant species ranges in Sikkilsdalen, central Norway. *Ecography* **35**, 922-932 (2012).
62 Telwala, Y., Brook, B. W., Manish, K. & Pandit, M. K. Climate-Induced Elevational Range Shifts and Increase in Plant Species Richness in a Himalayan Biodiversity Epicentre. *Plos One* **8** (2013).
63 Auer, S. K. & King, D. I. Ecological and life-history traits explain recent boundary shifts in elevation and latitude of western North American songbirds. *Global Ecol Biogeogr* **23**, 867-875 (2014).
64 Wolf, A., Zimmerman, N. B., Anderegg, W. R. L., Busby, P. E. & Christensen, J. Altitudinal shifts of the native and introduced flora of California in the context of 20th-century warming. *Global Ecol Biogeogr* **25**, 418-429 (2016).
65 Savage, J. & Vellend, M. Elevational shifts, biotic homogenization and time lags in vegetation change during 40 years of climate warming. *Ecography* **38**, 546-555 (2015).

Data availability

Source datasets are provided at https://datadryad.org/stash/share/cvQWOmBfKEki5GoHVkl-7yeOgRvAwkoEQquwEOl3wB4

Code availability

The code used for analysis can be found at https://datadryad.org/stash/share/cvQWOmBfKEki5GoHVkl-7yeOgRvAwkoEQquwEOl3wB4

Acknowledgements

We thank Y.-S. Chang and T.-C. Hiseh for helping process the topographical dataset; C.-H. Chen for providing statistical suggestion at the early stage of this study; C. Tomas, R. Childers, and C.-N. Chou for their comments on the early version of the manuscript. This work is funded by Ministry of Science and Technology, Taiwan (103-2621-B-001 -003 -MY3 and 101-2313-B-001 -008 -MY3 to S.-F. S.) and Academia Sinica (AS-SS-106-05 and AS-IA-106-L01 to S.-F.S.).

Author Contributions

S.-F.S. conceived the idea. S.-F. S., I.-C. C., and W.-P. C. designed the methodology. W.-P. C. performed the formal analysis. S.-F. S., I.-C. C., and W.-P. C. wrote the paper. All authors discussed results and provided input and edits on the manuscript.

Corresponding Author

Correspondence to I-Ching Chen and Sheng-Feng Shen.

Competing interests

The authors declare no competing interests.

Figures

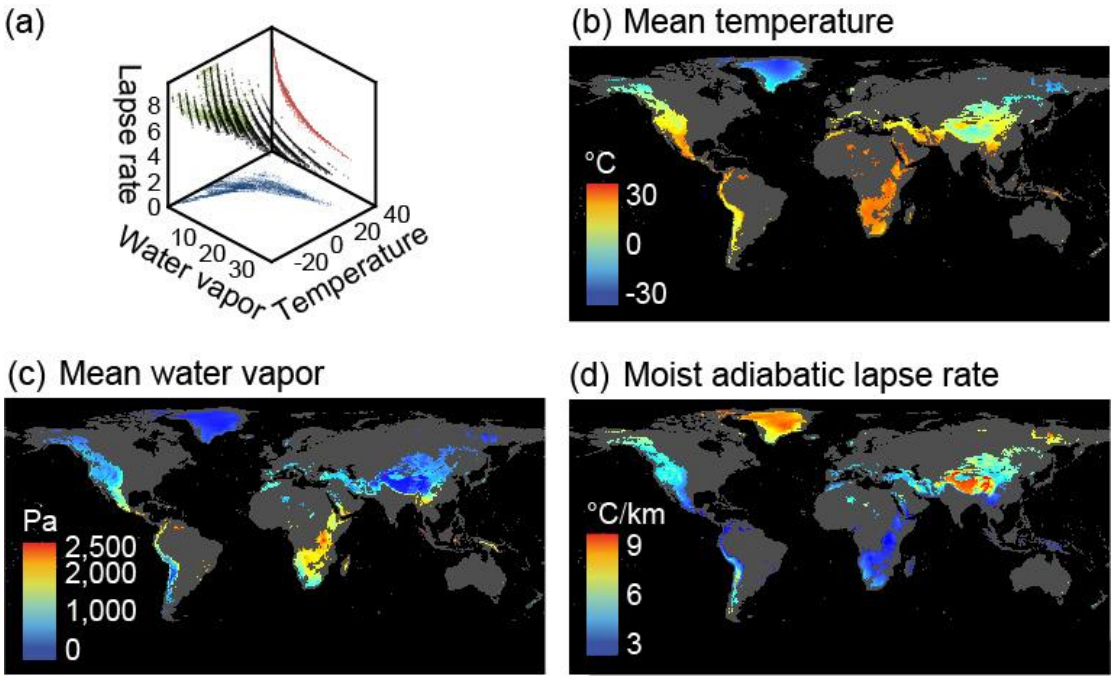

Figure 1| The foundation of moist adiabatic lapse rate for assessing climate velocity in global mountains. (a) The nonlinear effect of surface temperature and water vapor on lapse rate. The mean surface temperature (b) and water vapor (c) and derived mean moist adiabatic lapse rates (2011-2015) in global mountains (d).

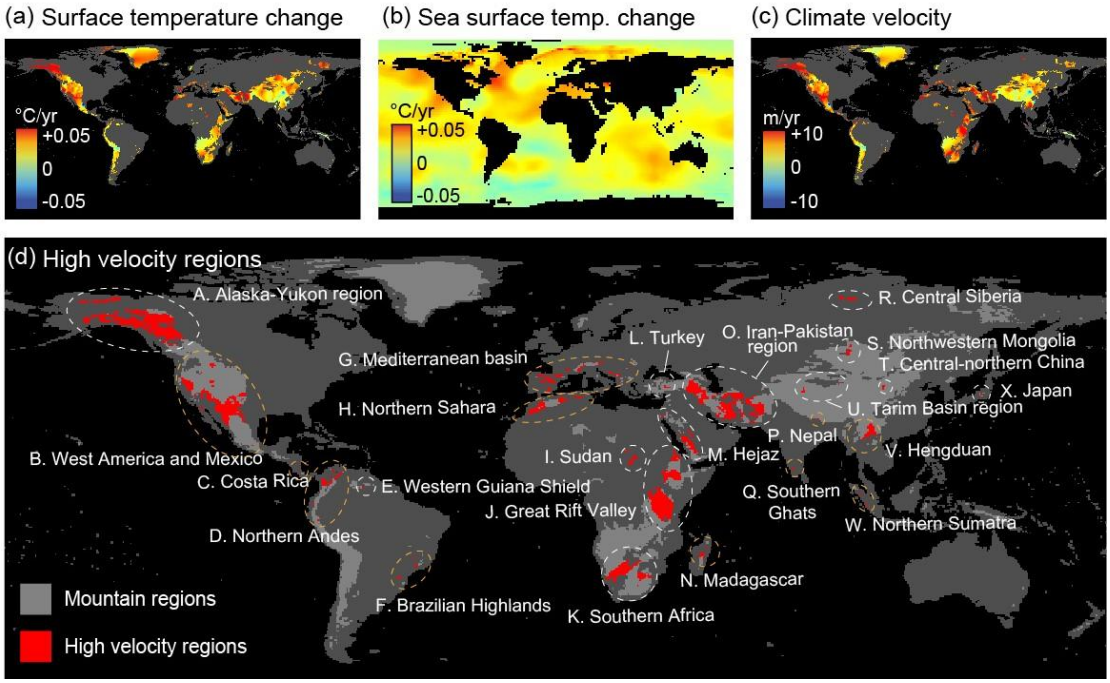

Figure 2|The velocity of climate change in global mountains from 1971 to 2015. Terrestrial (a) and sea (b) surface temperature change (1971-1975 V.S. 2011-2015) and derived elevational climate velocities in mountains (c). (d) The high climate-velocity mountains are defined as where the isotherms have shifted more than one standard deviation of the global mean value (higher than 8.45 m yr^{-1}).

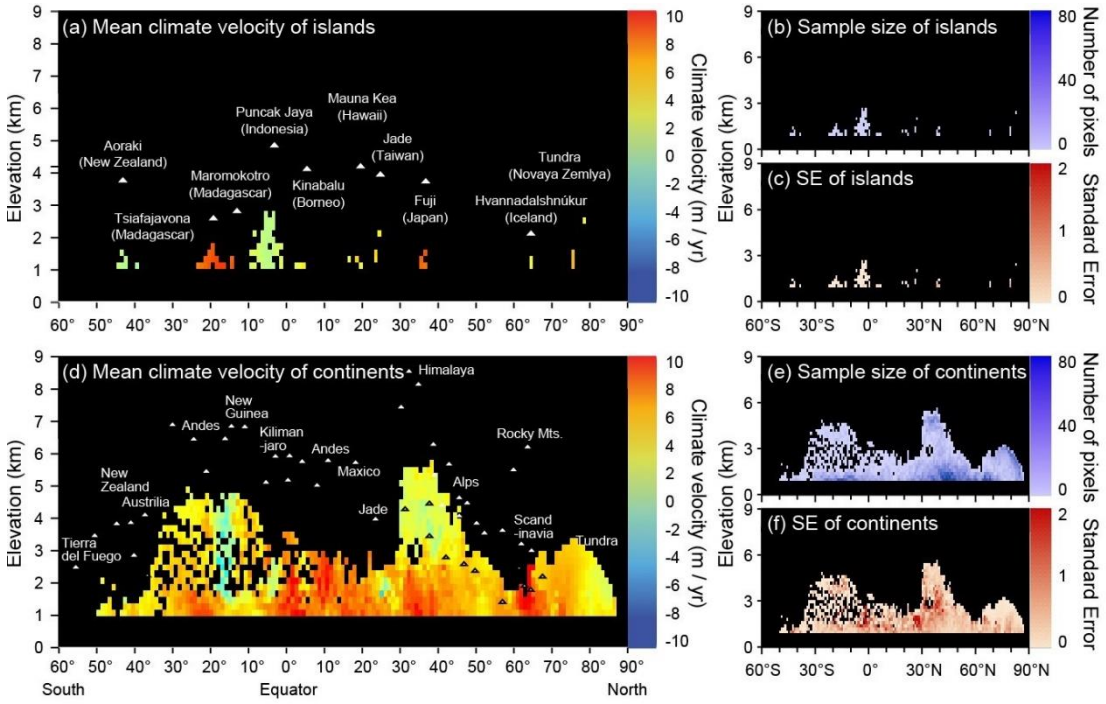

Figure 3| The velocity of climate change (1971-2015) in mountain islands (a, b, c) and along latitude-elevation gradients (d, e, f). Please see the Supplementary Method and Extended Data Fig. 3 for how to project a latitude-longitude map on a latitude-elevation map. Mountain summits are labeled for reference. Results that include the full 20th century (1901-2015) can be found in Supplementary Fig. 1 & 2.

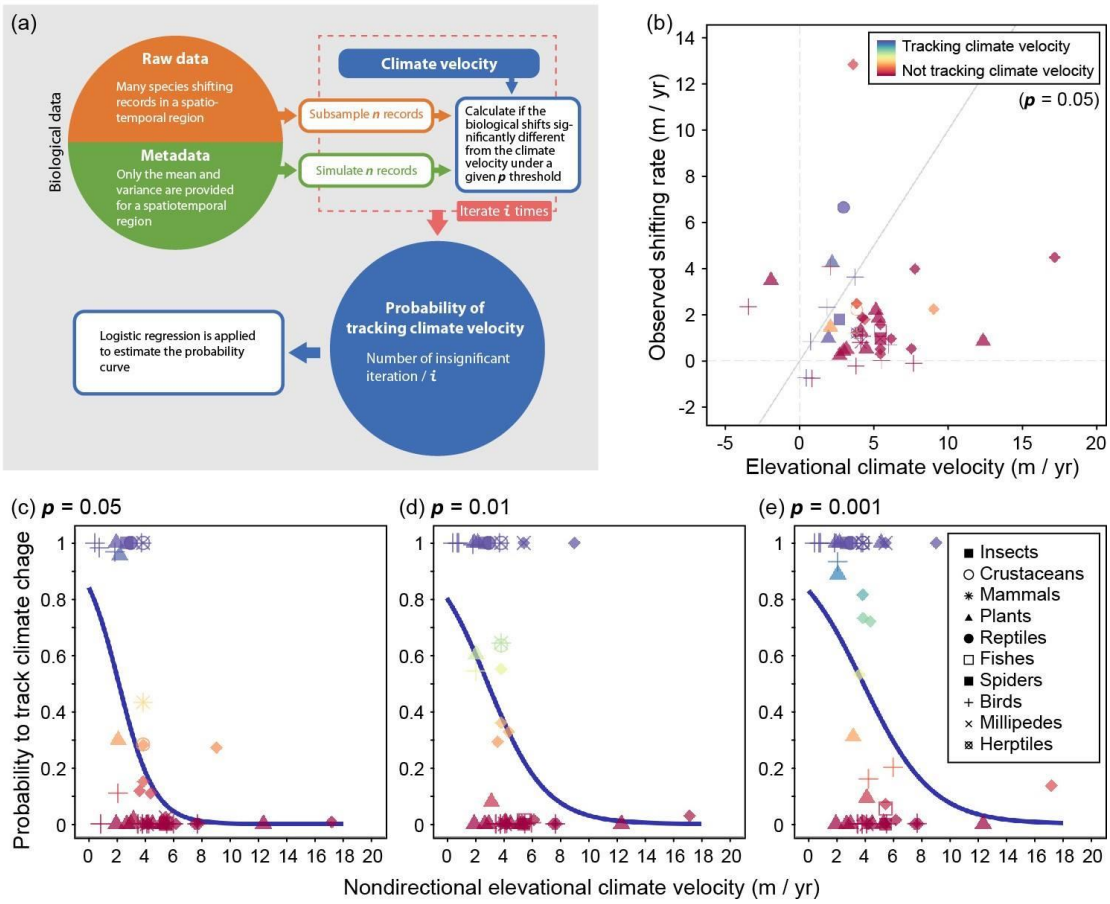

Figure 4|The probability of tracking climate velocities for mountain species. (a) The diagram summarizing how the probability of tracking climate velocities was calculated (i =1000) (b) The diagonal diagram for observed range shifts for mountain species and corresponding climate velocities. Blue labels represent cases that species track climate successfully (color-coded under p = 0.05 threshold). (c-e) The different probabilities of species tracking climate velocity under different p thresholds. Only mean values are shown here. Panel c-e share the same color legend with panel b. For raw data points, please see Extended Data Fig. 9 for details.

Additional information

Extended data figures and tables

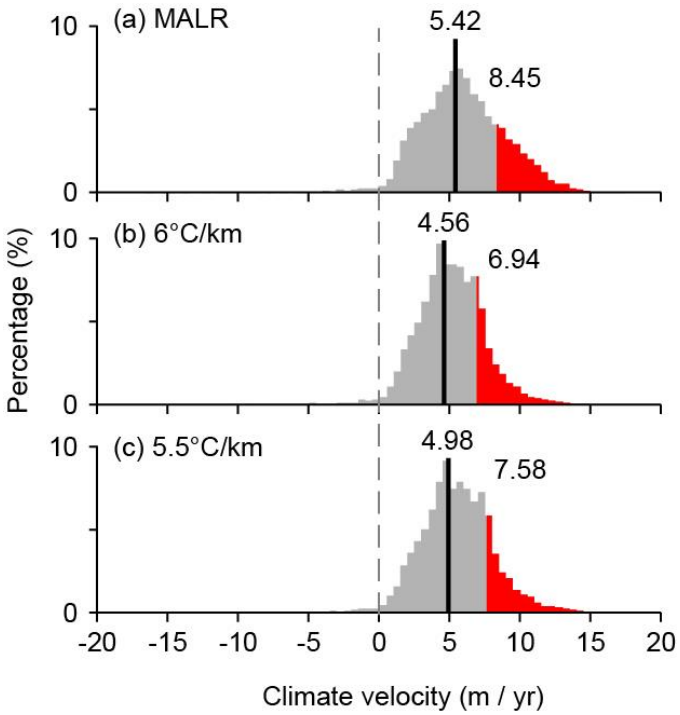

Extended Data Figure 1| Climate change velocity (1971-2015) derived from the MALR formula (a) and average lapse rates (b-c). (a) The histogram of MALR. **b-c**, Histograms derived from constant lapse rates 6°C km^{-1} **(b)** and 5.5°C km^{-1} **(c)**. The dashed and solid lines represent the zero velocity and the mean velocity, respectively. The red regions indicate the seriously warming regions (exceeding 1 standard deviation). The values labeled above the solid lines and red regions are the mean velocity and the minimum velocity of the seriously warming regions. The result of 20^{th} century (1901-2015) can be found in Supplementary Fig. 2.

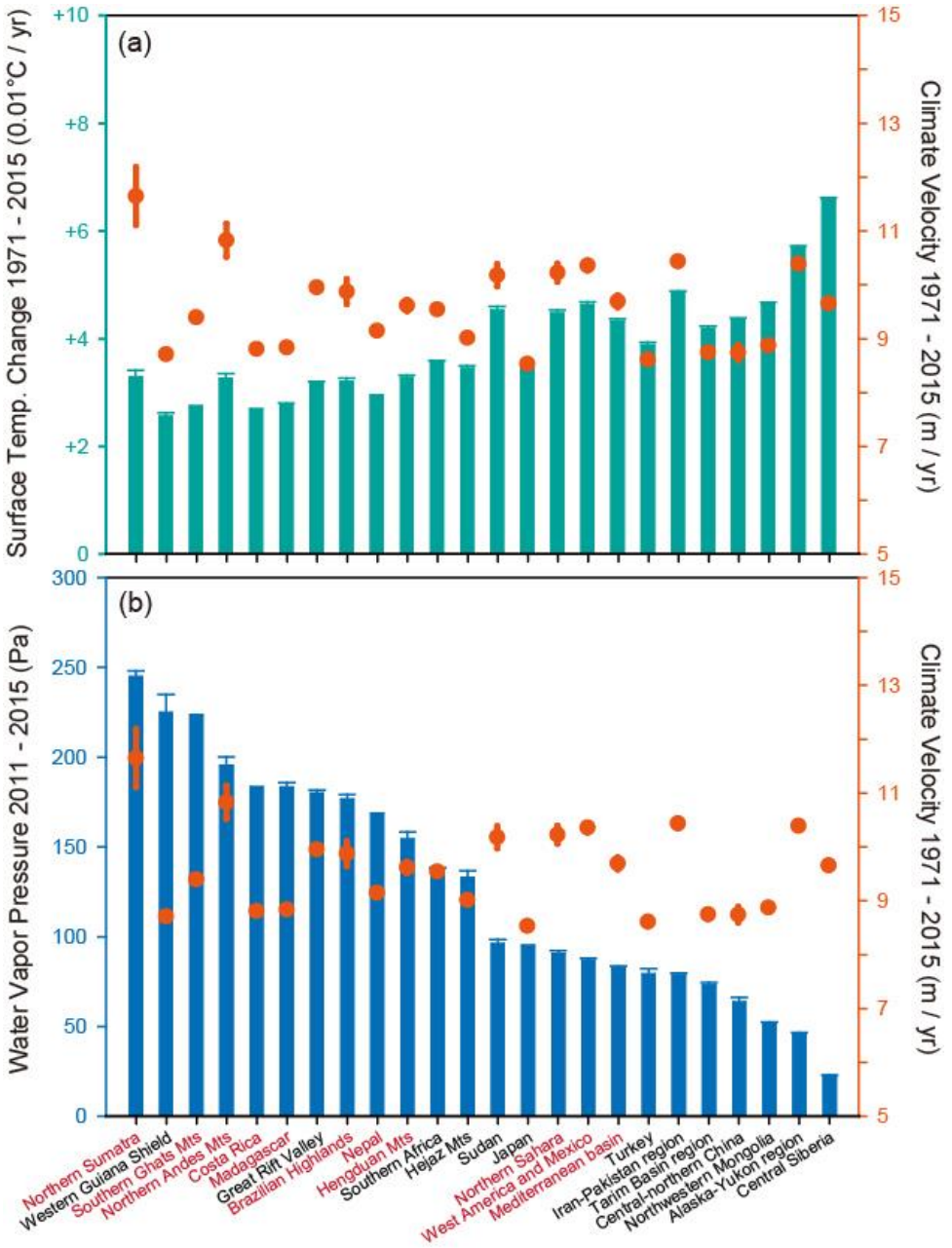

Extended Data Figure 2| The rising temperature and mean water vapor of the 17 high climate velocity regions in global mountains. For each region, orange dots denote the climate velocity (1971-2015), green bar represent surface temperature change (1971-1975 V.S. 2011-2015) (a); blue bars represent mean water vapor pressure (2011-2015) (b). Biodiversity hotspot regions are labeled in red. Detailed information on each region can be found in Supplementary Table 1 & Data availability section.

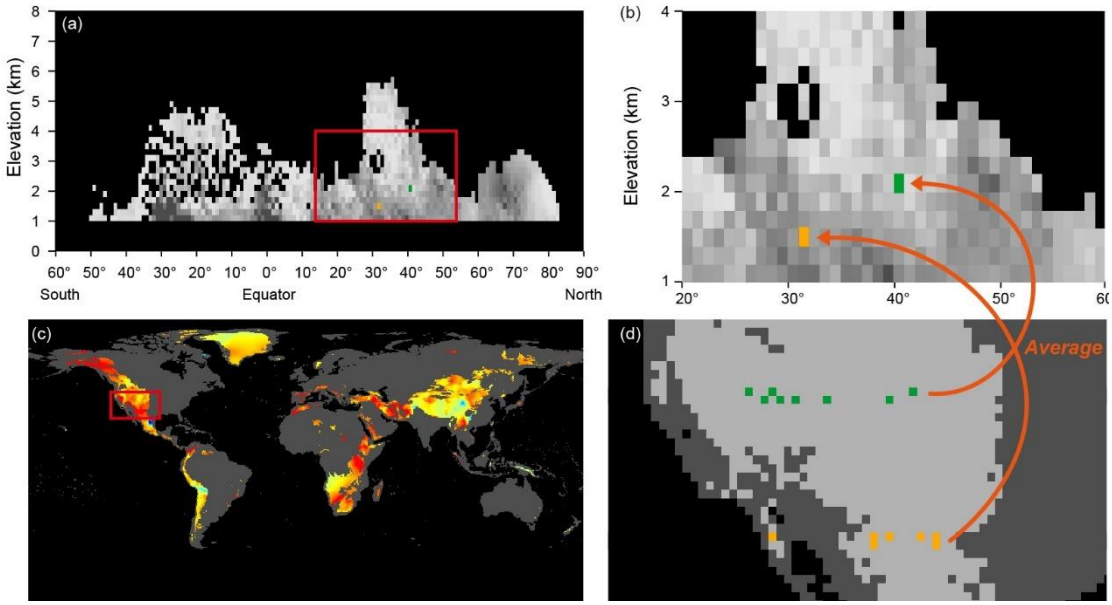

Extended Data Figure 3|Illustrations explaining how to project latitude-longitude maps onto latitude-elevation maps. (a) a gray-scale latitude-elevation map as Fig. 3b; the red box is shown in **b**. **(c)** a latitude-elevation map; the red box is shown in **d**. **(d)** The green pixels represent the latitudinal band of 40° and the altitudinal band of 2,000-2,200 m; yellow pixels represent the latitudinal band of 31° and the altitudinal band of 1,400-1,600 m. The green and yellow pixels in **d** are averaged to the green and yellow pixels in **b.**

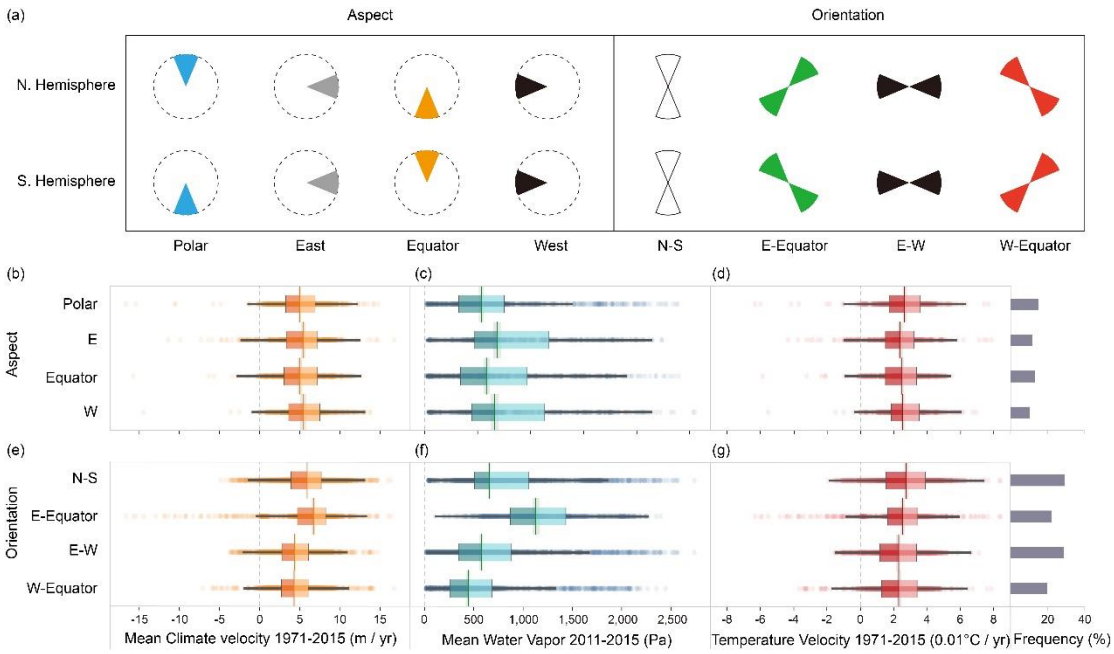

653

654

655 **Extended Data Figure 4| The definition mountain aspects and orientations (a)**
656 **and associated mean climate velocity (b,e), mean water vapor (c,f), temperature**
657 **change (d,g).** Median and its 95% confidence interval is shown at the center of each
658 box.

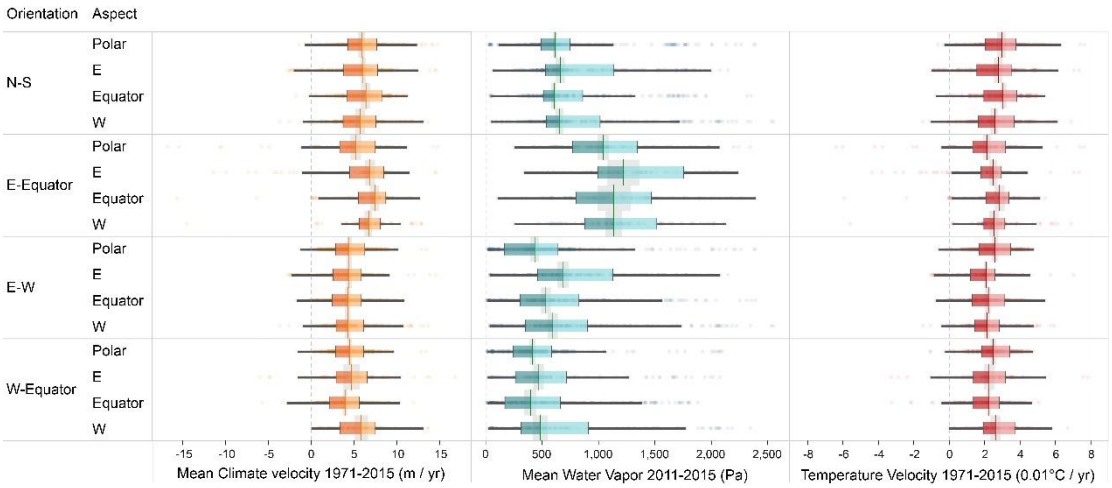

Extended Data Figure 5| Combined effect of mountain orientation and aspect on mean climate velocity, mean water vapor, and temperature change. Median and its 95% confidence interval is shown at the center of each box.

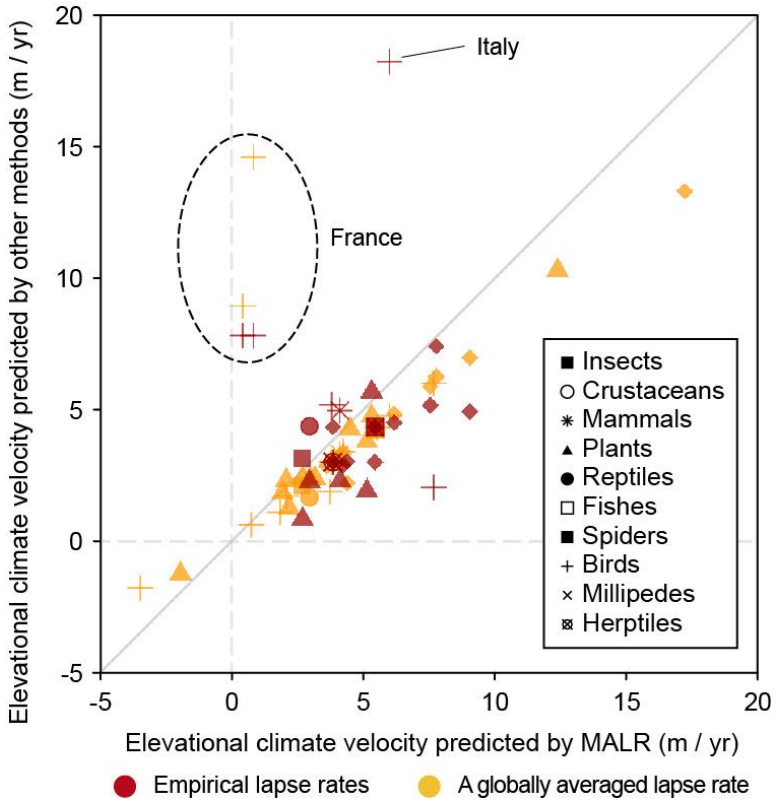

665

666 **Extended Data Figure 6| Comparison among elevational climate velocity derived**
667 **from MALR, a globally averaged lapse rate of 5.5 °C / km (yellow) and empirical**
668 **lapse rates in the original paper (red).** The regions of outliers are labelled.

669

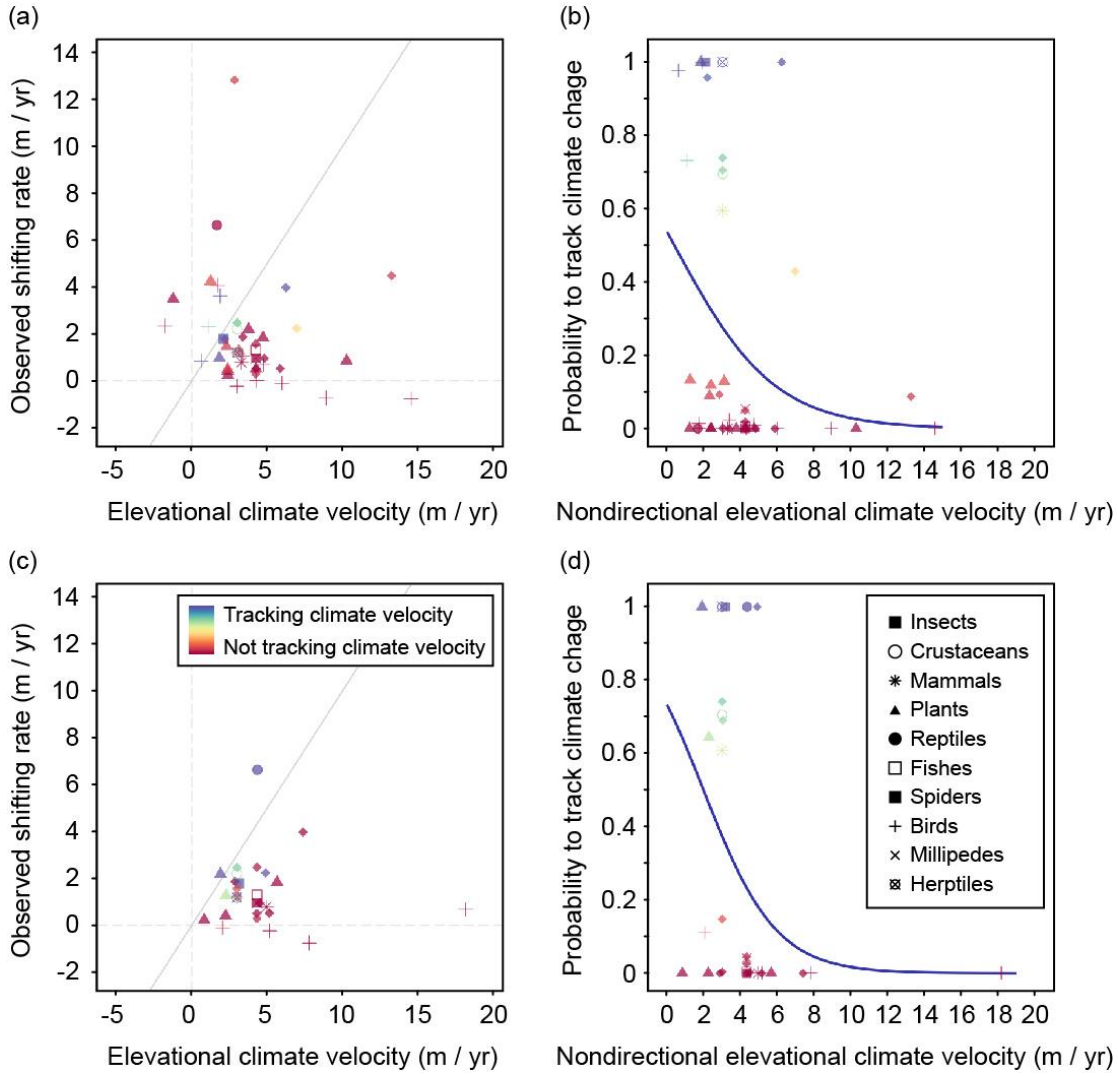

670

671 **Extended Data Figure 7| The maximum trackable climate velocity based on (a, b)**
672 **constant lapse rate (5.5 °C / km) and (c, d) empirical lapse rates in the original**
673 **paper.** The relationships between observed shifting rate and elevational climate
674 velocity are shown in **a** and **c**. Only mean values are shown here. The probabilities
675 that species may track climate velocity are shown in **b** and **d**.

676

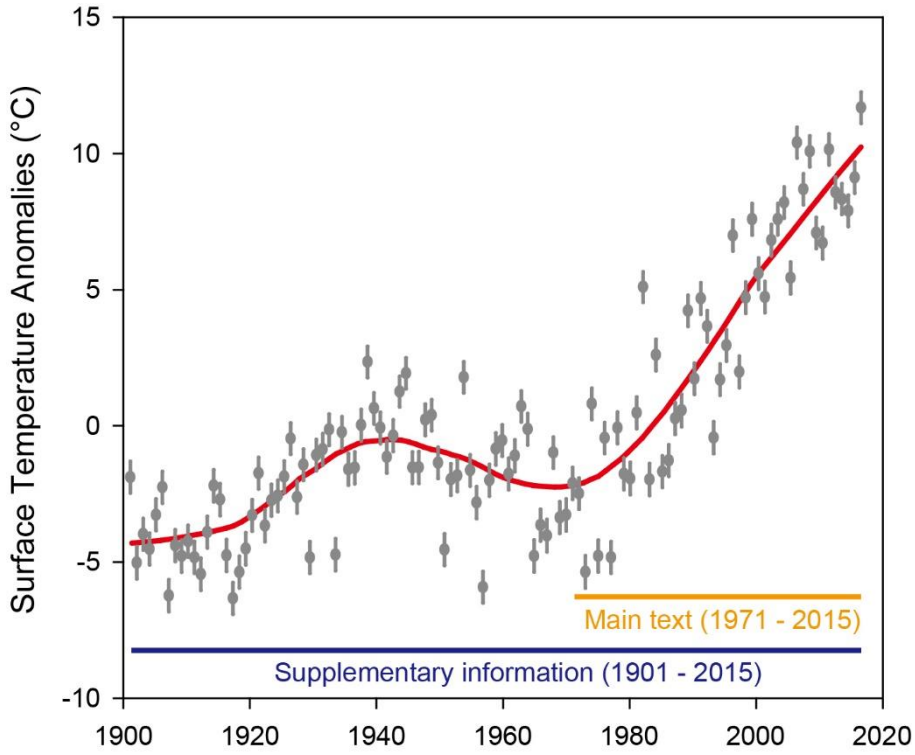

Extended Data Figure 8|The temporal extents we used in this study and an example explaining how we derived climate velocity through a period of time. The temperature trend from 1900 to 2015, and the target periods discussed in our main text and supplementary materials are labeled as orange and blue bars, respectively.

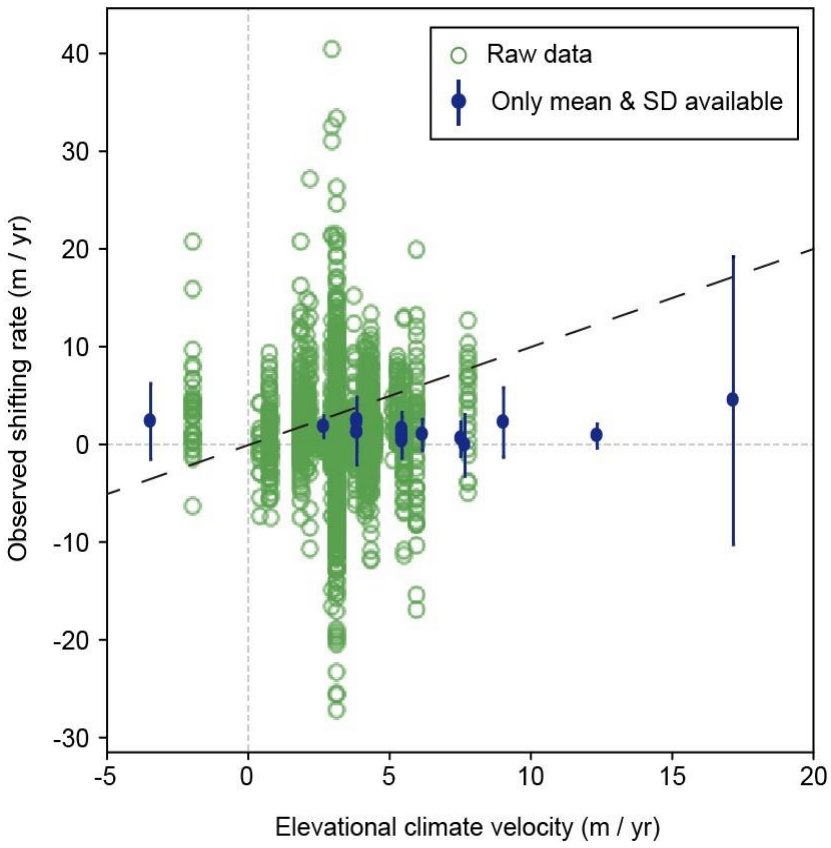

685

686

687 **Extended Data Figure 9|Raw biological data points used in our analyses.** All data
688 points from papers that provided raw data are shown (in green). Otherwise, mean and
689 standard deviation (reported in the original paper) are shown (in blue). Since a
690 proportion of original reports providing only mean and variance from a location, the
691 number of data points are highly overlapped. See Supplementary Table S2 for the
692 corresponding information and Data availability section for the dataset.

693

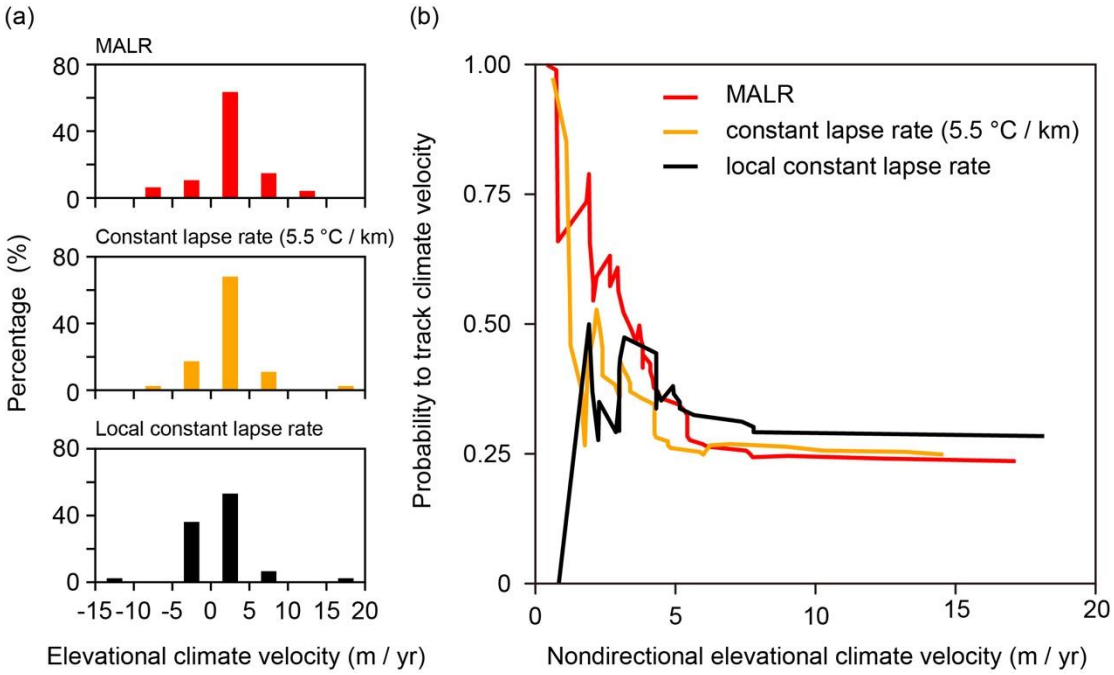

694
695

696 **Extended Data Figure 10| Residual frequency distribution and the probability of**
697 **climate tracking and climate velocity under different lapse rate calculations. (a)**
698 The residual frequency distribution simply derived from the difference between mean
699 of observed range shift velocity and predicted climate velocity. This result shows
700 clearly how better the climate velocity calculated by MALR, but it contains bias
701 because it compares only the mean value of observed records (ignoring the variance
702 of observed records). **(b)** an advanced analysis showing how climate velocity be
703 tracked under different lapse rate. Please see Supplementary Methods for details.

704

705

Supplementary information

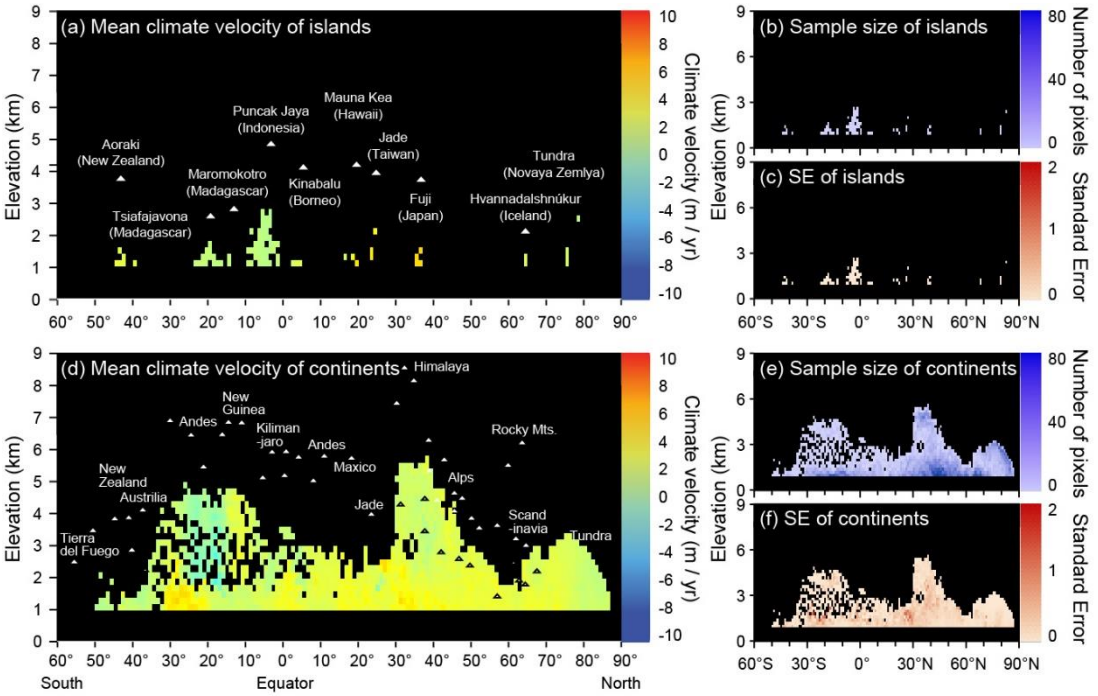

Supplementary Figure 1| Projections of the climate velocity (1901-2015) in global mountain regions of (a, b, c) islands and (c, d, e) continents. Please see the Supplementary Method and Extended Data Fig. 3 for how to project a latitude-longitude map on a latitude-elevation map. Some mountains are labeled as triangles. The sample size **(b, e)** and standard error **(c, f)** are shown.

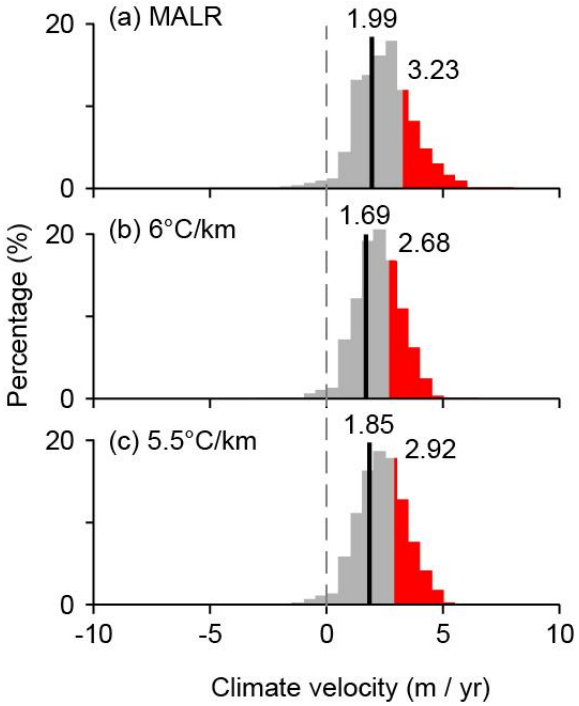

Supplementary Figure 2|Climate change velocity (1901-2015) derived from the MALR formula (a) and average lapse rates (b - c). (a) The histogram of MALR. **b-c**, Histograms derived from constant lapse rates 6°C km^{-1} **(b)** and 5.5°C km^{-1} **(c)**. The dashed and solid lines represent the zero velocity and the mean velocity, respectively. The red regions indicate the seriously warming regions (exceeding 1 standard deviation). The values labeled above the solid lines and red regions are the mean velocity and the minimum velocity of the seriously warming regions.

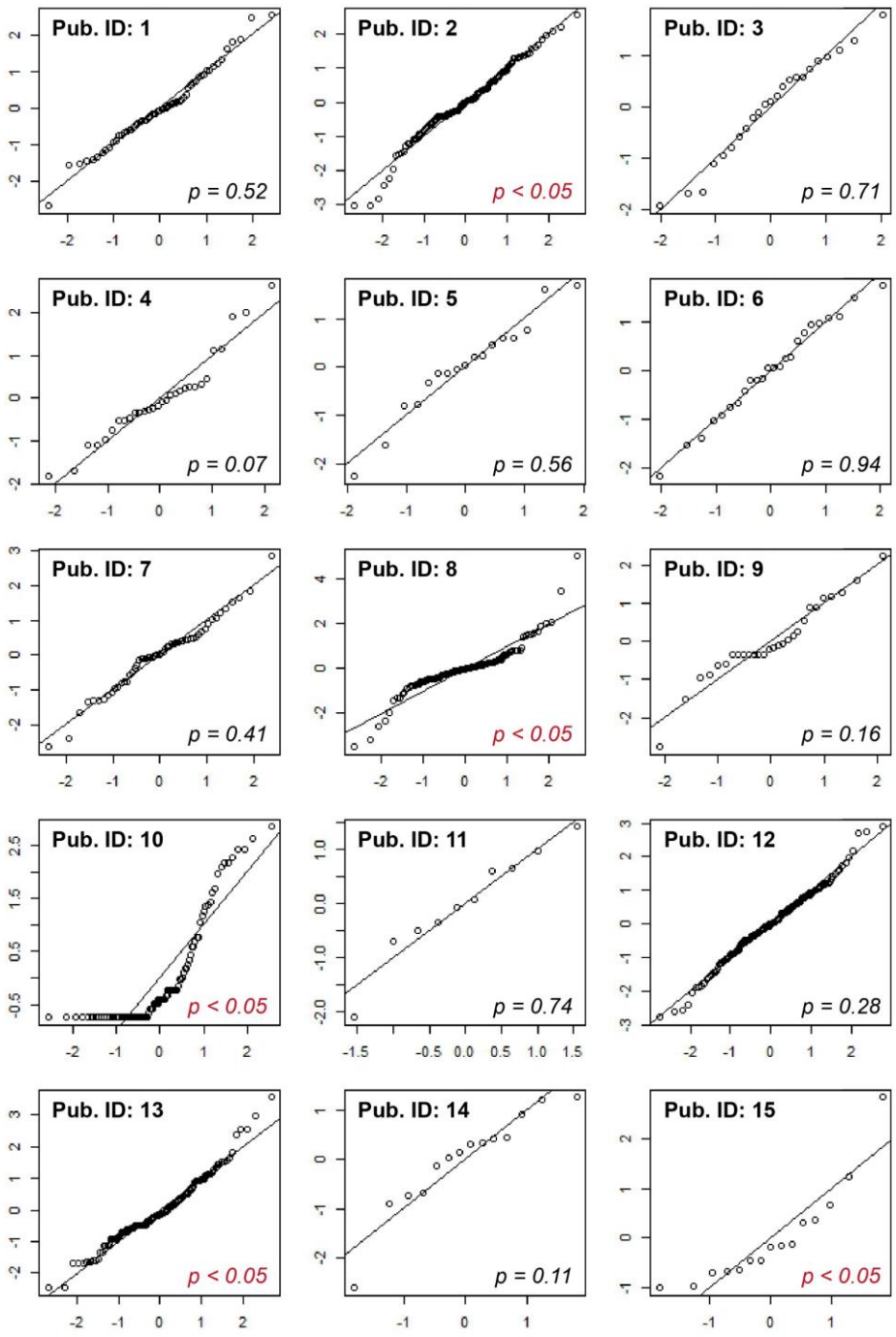

Supplementary Figure 3|Normality tests and qq plots for all biological raw datasets. Those datasets only reporting statistical summaries are not included. The p-values of Shapiro-Wilk normality tests for each dataset are shown in the lower-right corner of each panel.

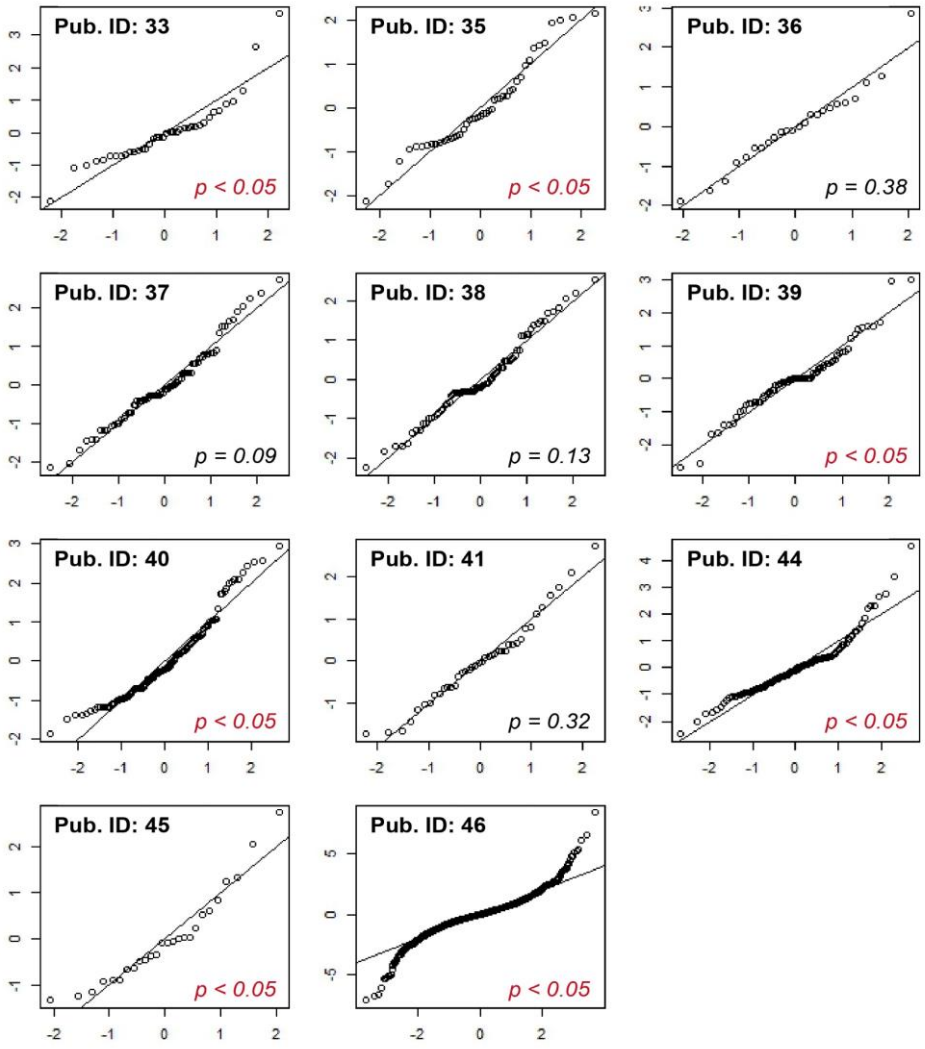

729

730 **Supplementary Figure 3| (Continued) the normality tests and qq plots for all**
731 **biological raw datasets.**

732

733

734 **Supplementary Table 1|Statistical information on major regions of high-velocity regions**

ID	Region	Area*	MALR† (2011-2015)		MAP‡ (1971-2015)		Water vapor§ (2011-2015)		Surface temp. change‖ (1971-2015)		Elevation¶		BD.# hotspot
A	Alaska-Yukon region	26.28	5.47	(0.02)	366.72	(8.71)	46.12	(0.38)	5.69	(0.04)	1299.29	(10.84)	N
B	West America and Mexico	14.84	4.46	(0.02)	349.98	(10.06)	86.86	(1.27)	4.63	(0.05)	1498.11	(19.44)	Y
C	Costa Rica	0.05	3.05	(NA)	3769.9	(NA)	183.27	(NA)	2.69	(NA)	1741	(NA)	Y
D	Northern Andes Mts	1.73	3.02	(0.03)	1718.4	(109.76)	195.09	(4.92)	3.26	(0.09)	1612.94	(63.36)	Y
E	Western Guiana Shield	0.15	2.93	(0.07)	2519.71	(387.52)	224.72	(10.19)	2.55	(0.07)	1125	(73.38)	N
F	Brazilian Highlands	0.54	3.24	(0.02)	1441.88	(24.15)	176.3	(2.78)	3.2	(0.07)	1108.55	(20.34)	Y
G	Mediterranean basin	3.75	4.46	(0.02)	770.9	(39.87)	82.56	(0.96)	4.32	(0.05)	1243.74	(29.71)	Y
H	Northern Sahara	3.16	4.38	(0.03)	295.7	(9.43)	90.47	(1.81)	4.47	(0.07)	1352.42	(40.95)	Y
I	Sudan	0.99	4.46	(0.05)	263.3	(28.35)	95.84	(2.63)	4.53	(0.07)	1104.4	(25.32)	N
J	Great Rift Valley	15.48	3.21	(0.01)	868.95	(16.03)	179.74	(1.75)	3.19	(0.02)	1451.66	(22.08)	N

K	Southern Africa	7.25	3.74	(0.03)	308.57	(12.9)	135.96	(2.33)	3.56	(0.03)	1180.22	(13.73)	N
L	Turkey	0.3	4.5	(0.05)	364	(13.17)	79	(3.26)	3.88	(0.06)	1445	(119.39)	N
M	Hejaz Mts	2.86	3.82	(0.06)	121.76	(5.58)	132.63	(4.04)	3.44	(0.06)	1259.76	(32.08)	N
N	Madagascar	0.69	3.16	(0.01)	1423.1	(73.13)	183.09	(2.74)	2.79	(0.01)	1231.71	(40.52)	Y
O	Iran-Pakistan region	17.11	4.66	(0.03)	221.42	(6.45)	78.46	(1.17)	4.85	(0.04)	1549.16	(21.03)	N
P	Nepal	0.05	3.23	(NA)	1616.12	(NA)	168.53	(NA)	2.96	(NA)	1467	(NA)	Y
Q	Southern Ghats Mts	0.1	2.92	(NA)	1054.4	(NA)	223.46	(NA)	2.75	(NA)	1199	(NA)	Y
R	Central Siberia	0.79	6.82	(0.03)	373.95	(5.87)	22.51	(0.4)	6.58	(0.04)	1092	(19.15)	N
S	Northwestern Mongolia	0.79	5.24	(0.02)	360.49	(24.49)	51.71	(0.81)	4.65	(0.02)	1233.13	(40.5)	N
T	Central-northern China	0.2	4.99	(0.07)	163.82	(7.25	63.58	(2.71	4.36	(0.02	1309.75	(83.26)	N
U	Tarim Basin region	0.39	4.78	(0.05)	64.66	(6.79)	72.78	(1.69)	4.18	(0.05)	1263.5	(19.17)	N
V	Hengduan Mts	2.27	3.4	(0.03)	1001.3	(19.89)	154.06	(4.25)	3.27	(0.05)	1538.5	(51.97)	Y
W	Northern Sumatra	0.25	2.82	(0.02)	2375.73	(239.68)	244.57	(3.34)	3.28	(0.14)	1122	(26.14)	Y
X	Japan	0.1	4.17	(NA)	1310.04	(NA)	95.09	(NA)	3.56	(NA)	1109.5	(NA)	N

* Percentage of each region divided by the total area of high-velocity regions in global mountains. (Unit: %)

† Moist adiabatic lapse rate derived from mean temperature and mean water vapor. (Unit: °C / km; format: mean [S.E.])

‡ Mean annual precipitation. (Unit: mm / yr; format: mean [S.E.])

§ Mean water vapor pressure; used as the parameter to derive MALR (2011-2015) in order to calculate climate velocity. (Unit: Pa; format: mean [S.E.])

‖ Temperature velocity. (1971-1975 V.S. 2011-2015; Unit: 0.01°°C /yr; format: mean [S.E.])

¶ Averaged elevation. (Unit: meter; format: mean [S.E.])

Biodiversity hotspot. This cell is filled by "Y" for any regions with biodiversity hotspots ([45]).

745 **Supplementary Table 2|Biological datasets.**

Pub_ID	Location	1st yr of 1st investigation	2nd yr of 1st investigation	1st yr of 2nd investigation	2nd yr of 2nd investigation	Taxon	Reference
1	Switzerland	1880	1920	1980	2005	Plants	[46]
2	Maylaysia(Mt. Kinabalu)	1965	1965	2007	2007	Insects	[2]
3	Spain (Sierra de Guadarrama)	1967	1973	2004	2004	Insects	[47]
4	Madagascar(Tsaratanana Massif)	1993	1993	2003	2003	Herptiles	[48]
5	France (Giffre valley)	1978	1980	2001	2002	Aves	[49]
6	France (Mont Ventoux alt.)	1973	1974	2000	2001	Aves	[49]
7	Italy (Alta Valsessera)	1992	1994	2003	2005	Aves	[50]
8	USA (New York State)	1980	1985	2000	2005	Aves	[51]
9	USA (Yosemite Nationa Park)	1914	1920	2003	2006	Mammals	[52]
10	Italy (Rhaetian Alps)	1954	1958	2003	2005	Plants	[53]
11	USA (Mt. Santa Rosa,CA)	1977	1977	2006	2007	Plants	[54]
12	West Europe (SW France)	1905	1985	1986	2005	Plants	[55]

13	Switzerland (12 Mts in Grisons)	1893	1893	2004	2004	Plants	[41]
14	Marion Island (sub-Antarctic)	1965	1966	2005	2007	Plants	[56]
15	Czech Republic	1951	1980	1995	2001	Insects	[57]
16*	UK (Great Britain)	1970	1982	2004	2005	Insects	[58]
17*	UK (Great Britain)	1970	1982	1995	1999	Insects	[37]
18*	UK (Great Britain)	1970	1980	1990	2000	Insects	[37]
19*	UK (Great Britain)	1960	1970	1985	1995	Insects	[37]
20*	UK (Great Britain)	1960	1970	1985	1995	Insects	[37]
21*	UK (Great Britain)	1965	1975	1990	2000	Insects	[37]
22*	UK (Great Britain)	1965	1975	1985	1995	Arachnids	[37]
23*	UK (Great Britain)	1965	1975	1990	2000	Insects	[37]
24*	UK (Great Britain)	1965	1975	1990	2000	Insects	[37]
25*	UK (Great Britain)	1965	1975	1990	2000	Millipedes	[37]
26*	UK (Great Britain)	1960	1970	1985	1995	Insects	[37]
27*	UK (Great Britain)	1965	1975	1990	2000	Arachnids	[37]

28*	UK (Great Britain)	1960	1970	1985	1995	Malacostraca	[37]
29*	UK (Great Britain)	1965	1975	1990	2000	Fishes	[37]
30*	UK (Great Britain)	1968	1972	1988	1991	Aves	[37]
31*	UK (Great Britain)	1960	1970	1985	1995	Mammals	[37]
32*	UK (Great Britain)	1960	1970	1985	1995	Herptiles	[37]
33	Peru	2003	2004	2007	2008	Plants	[59]
34*	Peru	1969	1969	2010	2010	Aves	[60]
35	Norway	1922	1932	2008	2008	Plants	[61]
36	Taiwan	1969	1969	2006	2006	Plants	[43]
37	USA (Lassen,CA)	1924	1928	2006	2007	Aves	[42]
38	USA (Yosemite,CA)	1915	1919	2003	2004	Aves	[42]
39	USA (Southern Sierra,CA)	1911	1911	2008	2009	Aves	[42]
40	India	1849	1850	2007	2010	Plants	[62]
41	USA	1977	1981	2006	2011	Aves	[63]

42*	France (South-western Alps)	1992	1993	2007	2007	Insects	[38]
43*	Spain (Sierra Nevada)	1981	1982	2006	2007	Insects	[38]
44	New Guinean (Mt. Karimui)	1955	1964	2002	2011	Aves	[8]
45	New Guinean (Karkar Island)	1959	1968	2002	2011	Aves	[8]
46	USA (California)	1895	1970	1971	2009	Plants	[64]
47*	Canada	1970	1970	2012	2012	Plants	[65]

746 * Only mean and variance/standard deviation/error are available from the literature

Supplementary Table 3|The probability of tracking climate velocity based on Wilcoxon signed-rank test under different sample sizes (n).

Pub_ID	n = 30	n = 40	n = 50	n = 60	n = 70	n = 80	n = 90	n = 100
1	0	0	0	0				
2	0.11	0.022	0.003	0	0	0	0	0
3	0							
4	1							
5	0							
6	1							
7	0	0	0					
8	0	0	0	0	0	0	0	0
9	0							
10	0	0	0	0	0	0	0	
11	0							
12	0.002	0	0	0	0	0	0	0
13	0	0	0	0	0	0	0	0
14	1							
15	0	0	0	0	0	0	0	0
16	0.271							
17	0							
18	0							
19	0.281333							
20	0							
21	0	0	0					
22	1							
23	0.024							
24	0.0033							
25	0.0227							
26	0.1507							
27	0	0	0	0	0	0		
28	0.2827							
29	0.0017							
30	0							
31	0.4327							
32	1							
33	0							

34	0	0	0					
35	0	0						
36	0.956							
37	0.983	0.989	0.999	1	1			
38	0	0	0	0	0			
39	0	0	0	0	0			
40	0.298	0.131	0.07	0.016	0.001	0	0	0
41	0.109	0						
42	0.006							
43	0.1177							
44	0.968	0.971	0.985	0.988	0.993	0.99	0.997	0.999
45	1							
46	0.016	0.005	0.001	0	0	0	0	0
47	0	0	0					

749

750

Figures

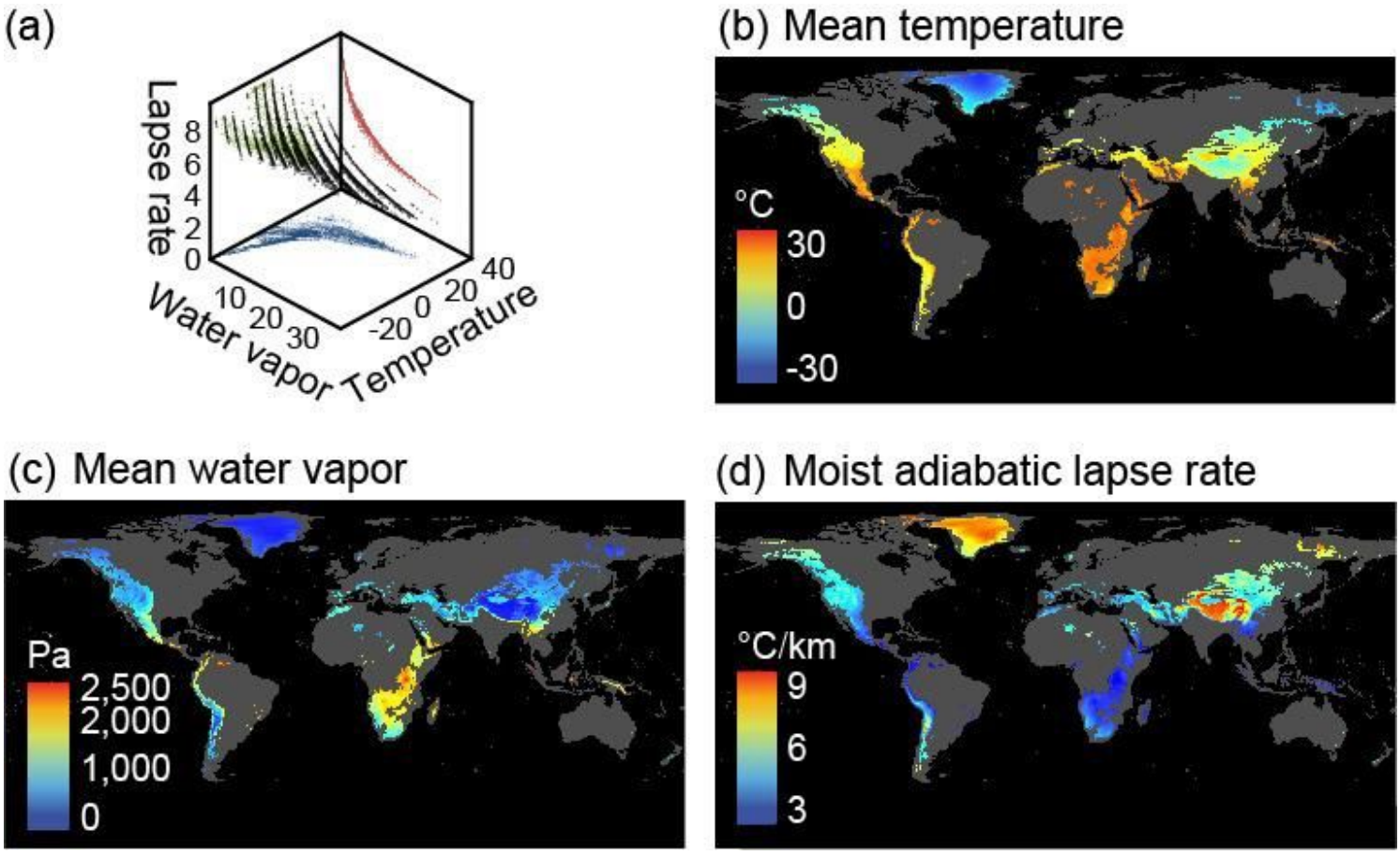

Figure 1

The foundation of moist adiabatic lapse rate for assessing climate velocity in global mountains. (a) The nonlinear effect of surface temperature and water vapor on lapse rate. The mean surface temperature (b) and water vapor (c) and derived mean moist adiabatic lapse rates (2011-2015) in global mountains (d). Note: The designations employed and the presentation of the material on this map do not imply the expression of any opinion whatsoever on the part of Research Square concerning the legal status of any country, territory, city or area or of its authorities, or concerning the delimitation of its frontiers or boundaries. This map has been provided by the authors.

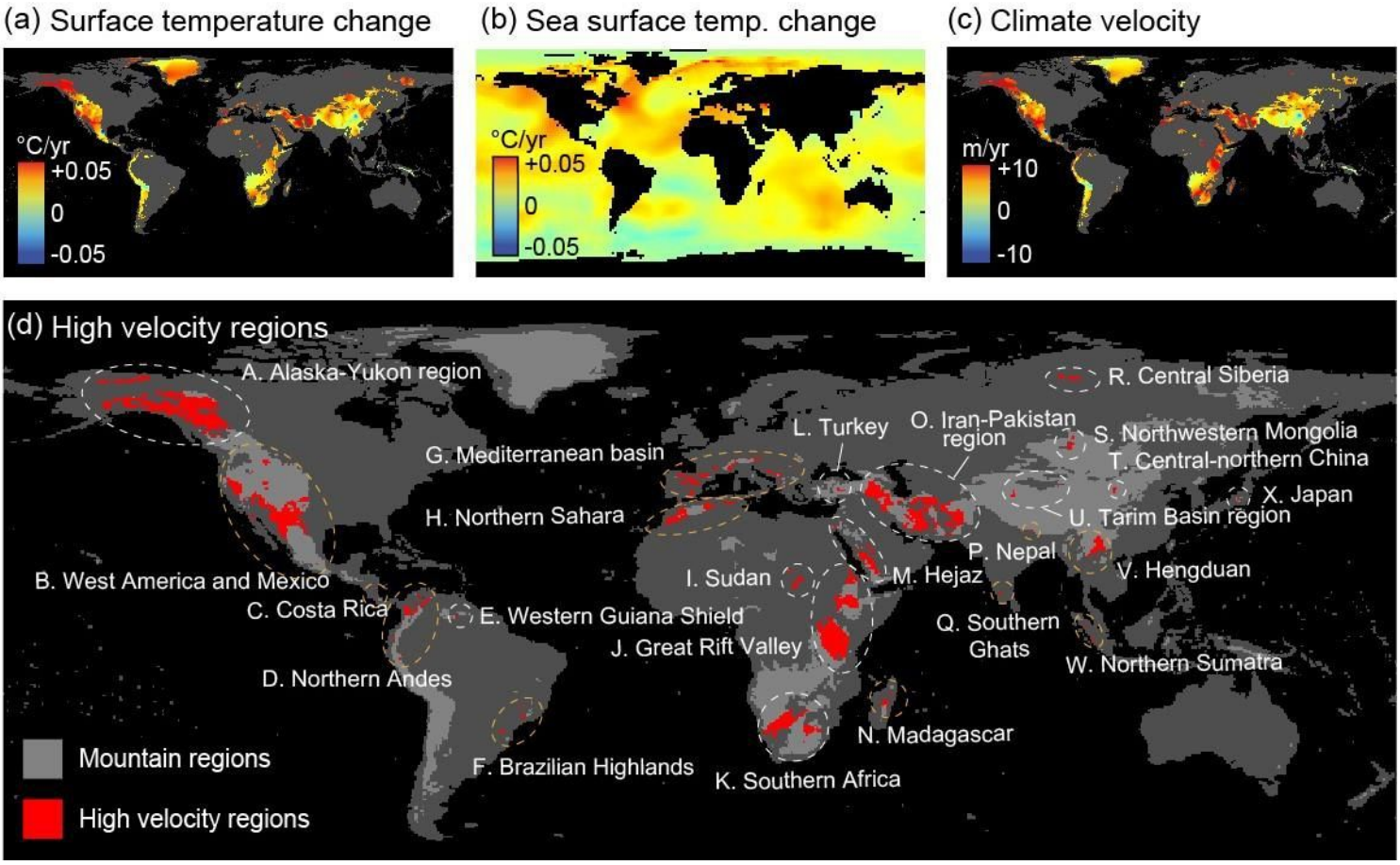

Figure 2

The velocity of climate change in global mountains from 1971 to 2015. Terrestrial (a) and sea (b) surface temperature change (1971-1975 V.S. 2011-2015) and derived elevational climate velocities in mountains (c). (d) The high climate-velocity mountains are defined as where the isotherms have shifted more than one standard deviation of the global mean value (higher than 8.45 m yr-1). Note: The designations employed and the presentation of the material on this map do not imply the expression of any opinion whatsoever on the part of Research Square concerning the legal status of any country, territory, city or area or of its authorities, or concerning the delimitation of its frontiers or boundaries. This map has been provided by the authors.

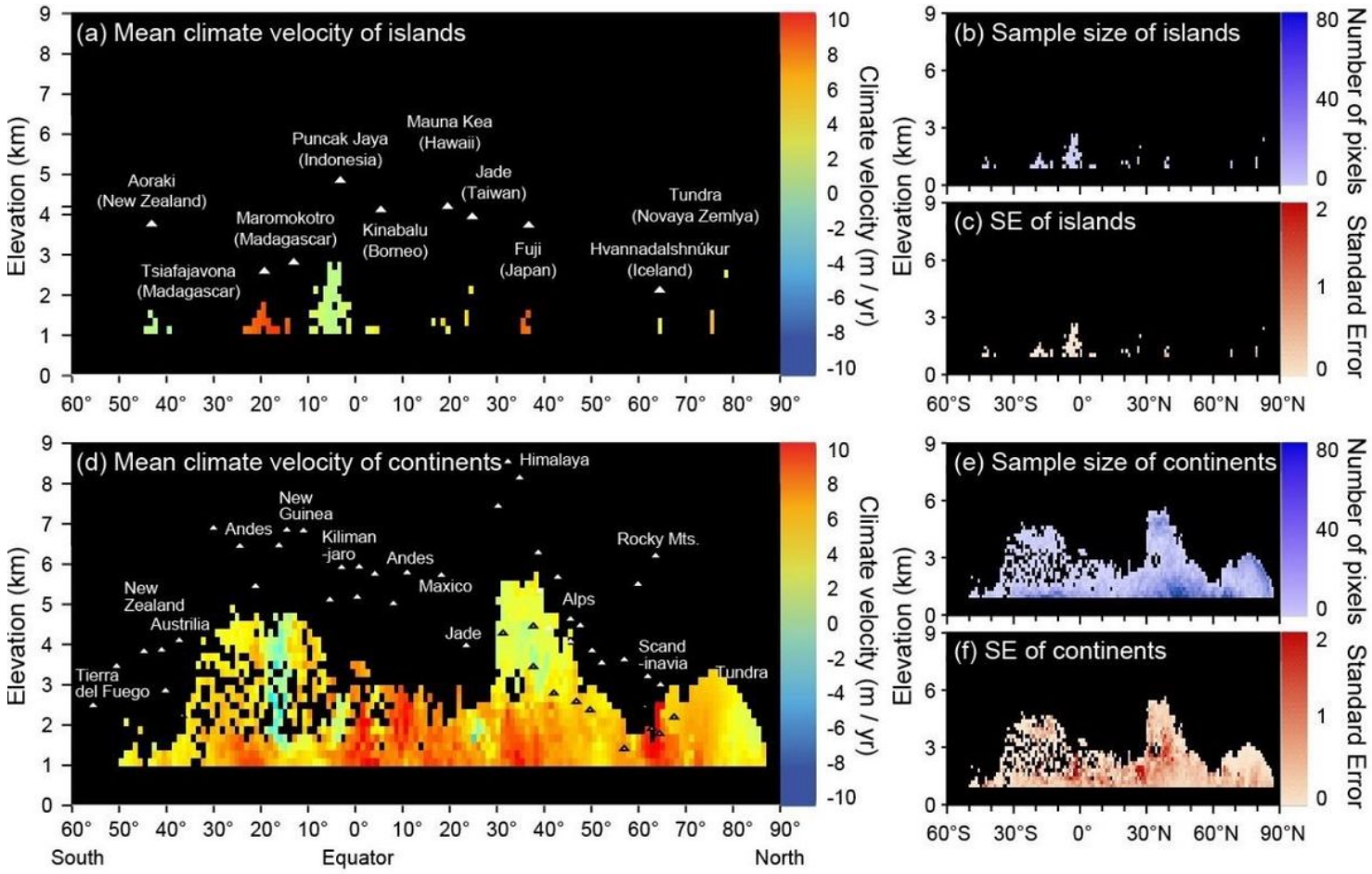

Figure 3

The velocity of climate change (1971-2015) in mountain islands (a, b, c) and along latitude-elevation gradients (d, e, f). Please see the Supplementary Method and Extended Data Fig. 3 for how to project a latitude-longitude map on a latitude-elevation map. Mountain summits are labeled for reference. Results that include the full 20th century (1901-2015) can be found in Supplementary Fig. 1 & 2.

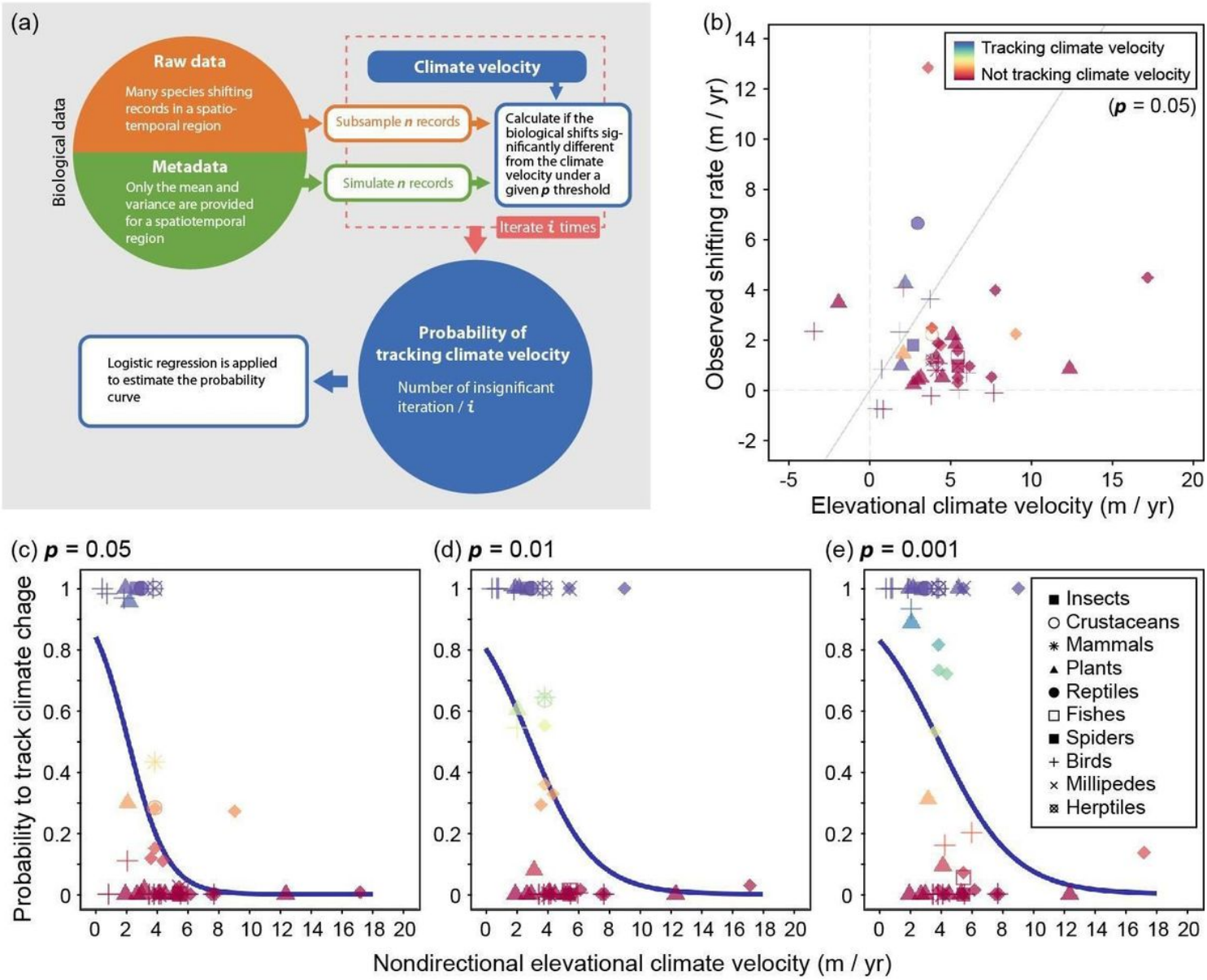

Figure 4

The probability of tracking climate velocities for mountain species. (a) The diagram summarizing how the probability of tracking climate velocities was calculated (i =1000) (b) The diagonal diagram for observed range shifts for mountain species and corresponding climate velocities. Blue labels represent cases that species track climate successfully (color-coded under p = 0.05 threshold). (c-e) The different probabilities of species tracking climate velocity under different p thresholds. Only mean values are shown here. Panel c-e share the same color legend with panel b. For raw data points, please see Extended Data Fig. 9 for details.